SLM
Soil Physics and
Land Management

Using Sentinel-1 and field measurements to evaluate LISEM performance in Catsop, South Limburg

MSc thesis by Theo Fonville

June 2020

Soil Physics and

Land Management Group

WAGENINGEN UNIVERSITY
WAGENINGEN UR

Master thesis Soil Physics and Land Management Group submitted in partial fulfilment of the degree of Master of Science in International Land and Water Management at Wageningen University, the Netherlands

Study program:
MSc International Land and Water Management

Student registration number:
960223243070

Supervisors:
WU Supervisors: dr. ir. JEM Baartman & MC Commelin MSc

Examiner:
Dr. ir. M.J.M.P. Riksen

Date:

13/07/2020

Soil Physics and Land Management Group, Wageningen University

Table of contents

1. Introduction and research questions

Throughout the world erosion is a problem of considerable proportion (Rodrigo Comino, et al., 2016). Erosion by wind or water detaches soil particles, which are deposited elsewhere. This process leads to fertile topsoil being washed away. Not only does this lead to soil loss at the higher located parts on a slope, it also causes the soil to be deposited elsewhere, often at an inconvenient place such as in a village, on a road or in a reservoir. Soil erosion models (SEMs) have been used as a tool to understand and predict soil erosion on both short- and long-term scales (Baartman et al., 2013; Schoorl, Veldkamp, & Bouma, 2002; Coulthard, Hancock, & Lowry, 2012). SEMs use inputs such as a digital elevation model (DEM), the amount and intensity of rainfall and soil characteristics to predict the amount and location of soil erosion and runoff for a certain rainfall event. These models are often event-based, meaning that they require input for a certain rainfall event and give according output. These models can be used to estimate the effect of a rainfall event on a landscape with reasonable accuracy (Pandey, Himanshu, Mishra, & Singh, 2016). This is potentially crucial information in landscapes that are not flat, such as the study area of this research, South Limburg (van der Velde et al., 2018). During rainfall events, erosion of soil in the higher parts of the landscape can lead to mudflows in the lower parts. Knowing the spatial patterns and quantity of soil erosion can be vital information in preventing mudflows in populated areas. LISEM (Limburg Soil Erosion Model) is an example of an event-based SEM able to calculate runoff and the amount of sediment for a given rainfall event. Usually, the model is calibrated by adjusting parameters such as erodibility, deposition or hydraulic conductivity (Baartman et al., 2013). LISEM uses different input parameters to process and calculate erosion and runoff. Some of these parameters, like hydraulic conductivity and Manning's N, change model output more than others (Sheikh et al., 2010; Kvaerno & Stolte, 2012).

Modern technologies like satellite observations are becoming more and more accessible for scientific purposes. Satellites monitor the earth constantly and mostly at fairly high resolutions, providing previously unparalleled spatiotemporal coverage of soil and crop characteristics. The Sentinel-1 satellite has been used for soil moisture mapping at lower resolutions (El Hajj et al., 2017). Recently, research has suggested and successfully implemented higher resolution use of Sentinel-1 (Hornaek et al., 2012 & Lozach et al., 2020). An ongoing research project in the Netherlands successfully applied Sentinel-1 to create a soil moisture monitoring network in the eastern part of that country (Benninga et al., 2018). This methodology could also possibly be used to create soil moisture maps for SEMs such as LISEM.

Until now, both the hydraulic conductivity and initial soil moisture parameters of LISEM are often estimated or sampled and interpolated, but this does not always result in accurate values (Rousseau et al., 2012). Since the model can be used as a tool to model landscape runoff behaviour, accurate values are crucial. Because erosion causes a lot of nuisance in South Limburg, accurate modelling can help predict where sedimentation will occur (Schouten, Rang, & Huigen, 1985; Hollis, 1975; Winteraeken & Spaan, 2010). This in turn can help to design measures to prevent or mitigate this. Because LISEM is quite sensitive to both initial soil moisture content and hydraulic conductivity, improvement of input data for initial soil moisture content consequently could improve model output (Sheikh et al.,2010). At the moment, no research has been done into the effects of improved initial soil moisture content and hydraulic conductivity spatial values on model output. This research aimed to investigate whether the accuracy of initial soil moisture content and hydraulic conductivity values can be improved and if this leads to an improvement in LISEM output accuracy. The main question of this research was therefore formulated as: to what extend can different ways of data collection for initial soil moisture content and hydraulic conductivity help improve LISEM infiltration

maps accuracy and consequently LISEM output? The first sub question that was answered is: to what extend can existing soil moisture sensors and manual sampling provide a reference to create accurate satellite obtained soil moisture maps? The second question will be: to what extend can satellite obtained soil moisture values produce significant improvement to model output? Finally, the research will focus on to what extend manually obtained hydraulic conductivity maps can produce significant improvement to model output?

2. Study area

The study area is located in the Limburg, the southern part of the Netherlands, see figure 1.

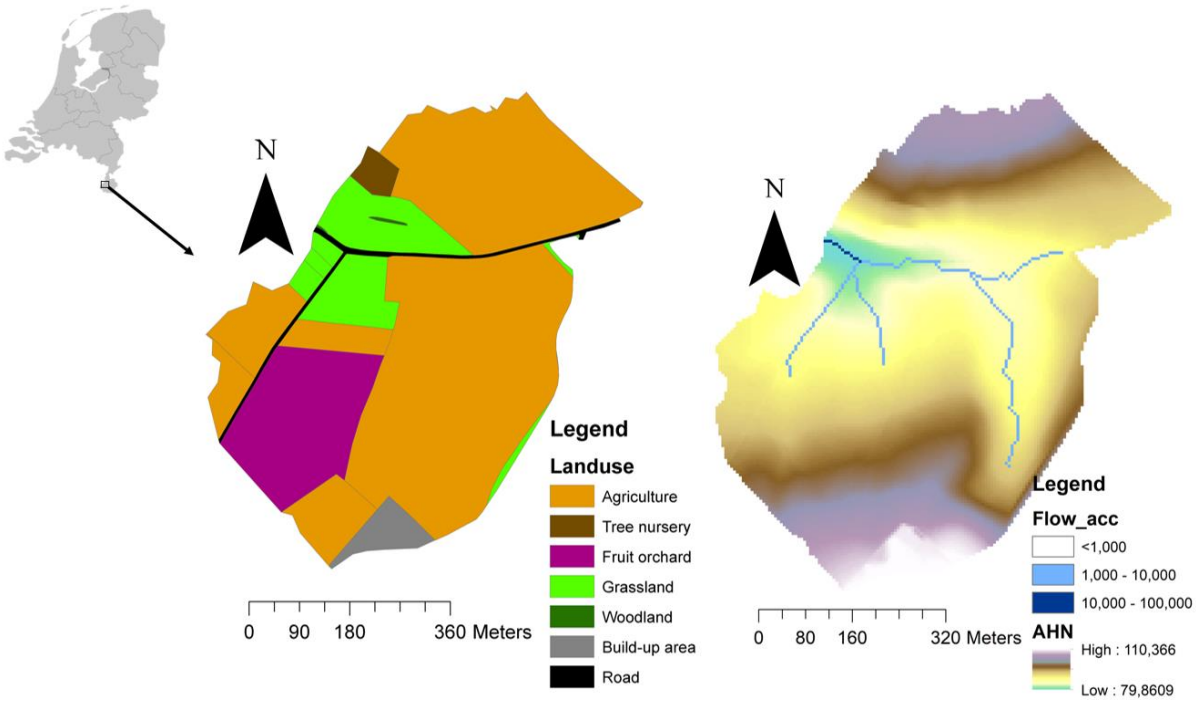

Figure 1: Location of research area in the Netherlands (top left), land use (left) and digital elevation model with stream network (right)

The coordinates of the study area are 50.93°N and 5.78°E. The climate in this part of the Netherlands features mean daily temperatures ranging from three degrees during winter to roughly twenty degrees during summer. The yearly precipitation is around 750mm with the wettest months being June, July and August with a precipitation of around 75 mm per month (KNMI, 2020). The type of rainfall also differs throughout the year. During winter and spring almost all showers are relatively longer and less intensive. Especially during summer, but also sometimes in autumn, showers tend to be shorter and more intensive, producing more runoff.

The soil in the catchment is, like the rest of southern Limburg, loess soil. This soil type has a grain size of around 50-60µm (Heinen, Bakker, & Wösten, 2018). The land use in the catchment is predominantly agricultural. As can be seen in figure 1, the two largest fields are agricultural fields. In 2019, the main agricultural field was planted with potatoes. During autumn and winter, the northern agricultural field was covered in yellow mustard. When potatoes are grown on the fields, ridges are made parallel to the contour lines (in figure 1 that means ridges with a west-northwest direction). Some ridges at the western part of the main agricultural field are perpendicular to the contour lines. There are two apple orchards which are permanent considering this study's time frame. Between the apple trees are grass strips. Furthermore, there are some plots of grass in the catchment.

3. Background

3.1 – Sentinel 1

The Sentinel 1 satellite that was used for this research is part of the ESA's Copernicus Programme. It collects *'C-band synthetic aperture radar (SAR) imagery at a variety of polarizations and resolutions'* (Google, 2020). With this, Sentinel is part is part of the active remote sensing, meaning it sends a signal of its own rather than using for example radiation from the sun as basis of observations. This has some advantages and disadvantages. One of the advantages is that microwave SAR imagery can penetrate through not too thick cloud layers and vegetation. Another advantage that obviously comes with all active remote sensing is that it is also possible to take images at night. There are also some disadvantages, starting with interpretation of data. (Pre)processing of data is required since the raw data collected in this way are harder to interpret than optical (passive) remote sensing data. Another disadvantage is the occurrence of speckle effects in the image. When using satellite imagery, it is important to determine and realize some key parameters of the satellite observations: wavelength, polarization and incidence angle.

3.1.1 – Wavelength

The wavelength of a signal depends of its frequency. A higher frequency means a shorter wavelength and less capability to radiate through materials and vice versa. Lower frequency (and therefore longer wavelength) bands are therefore used in for example ground penetrating radar because of their capabilities to penetrate through materials.

As mentioned before, Sentinel 1 collects C-band data. A band actually is a range of certain frequencies that can be used for certain purposes. As can be seen in table 1, different frequencies can be used for different applications.

Table 1: Overview of satellite bands, according frequencies and application examples. Edited from: (Podest, 2017)

Band	Frequency range	Application examples
L-band	1 – 2 GHz	Agriculture, forestry, deeper soil moisture
C-band	4 – 8 GHz	Agriculture, surface soil moisture
X-band	8 – 12 GHz	Agriculture and high resolution radar
Ku-band	14 – 18 GHz	Glaciology and snow cover mapping
Ka-band	27 – 47 GHz	High resolution radars

3.1.2 – Polarization

There are four polarizations within the Sentinel 1 satellite: horizontal transmit, horizontal receive (HH), horizontal transmit, vertical receive (HV), vertical transmit, horizontal receive (VH) and vertical transmit, vertical receive (VV). For this study, the VV polarization was used. It is not within the scope of this study to explain and elaborate on the choice in technical terms. The VV polarization was chosen because it is the most used over land and is more sensitive to soil moisture than VH (Benninga & Pezij, 2019).

3.1.3 – Incidence angle and backscatter

The incidence angle is the angle between the surface on which the radar illuminates and the direction of the illumination beam. The angle will slightly change based on the height of the sensor (satellite) and the orbit of the sensor. The backscatter of the radar contains information about the surface which it illuminates. Calm open water and paved highways for example cause a low backscatter because of their dielectric properties – they are good reflectors. In SAR images it is

therefore displayed as a darker colour. Built-up areas, rough surfaces and vegetation cause a higher backscatter, as can be seen in figure 2 and are therefore displayed as more bright (white) areas on the SAR images. In figure 2a, the surface reflects the signal without backscatter (think of water or concrete). Figure 2b shows what happens on a rough surface, the reflection is in multiple directions and only part is reflected back to the emitter. More or less the same happens in figure 2c. These figures are examples of build-up area and vegetation respectively.

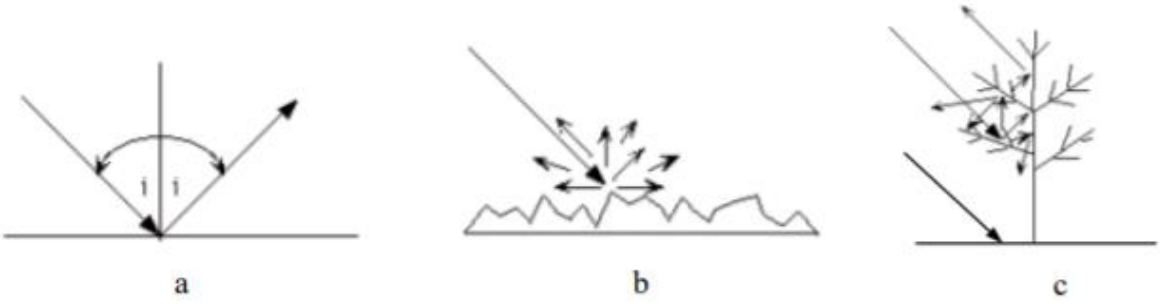

Figure 2: Backscatter mechanisms. Source: Chang (2016)

3.2 – The Limburg Soil Erosion Model (LISEM)

As mentioned before, LISEM is a SEM. More specific it is a physically based model which is capable of simulating rainfall events and the erosion and runoff that they cause. LISEM works event-based and is not designed to model long-term impact. As can be seen in figure 3, part of the main loop of LISEM is calculating infiltration through calculating precipitation and interception first. The infiltration component of LISEM is based on soil properties, roads and buildings. The soil properties consist of hydraulic conductivity (Ksat), porosity (theta-s) and initial soil moisture content (theta-I) (Jetten, 2018).

3.2.1 – Hydraulic conductivity

The hydraulic conductivity (Ksat) of a soil had a unit of distance/time (e.g. mm/hour). It refers to the soil property of how much water can infiltrate in the soil in a certain time in saturated condition. The higher the hydraulic conductivity, the higher the potential flow through the soil and the more water can infiltrate into the soil during a rain storm. Soil with a higher hydraulic conductivity are for example sandy soils. Lower hydraulic conductivity is found in soils that have smaller grain sizes, such as loess and clayish soils.

3.2.2 – Porosity

The porosity (theta-s) is defined as the amount of space in a soil that is available to store water. For example, a porosity of 0.5 means that 50% of the soils' volume is available for water storage. The soil cannot store more water than the porosity. Therefore, if the porosity value is reached, water will no longer be able to infiltrate and start producing runoff.

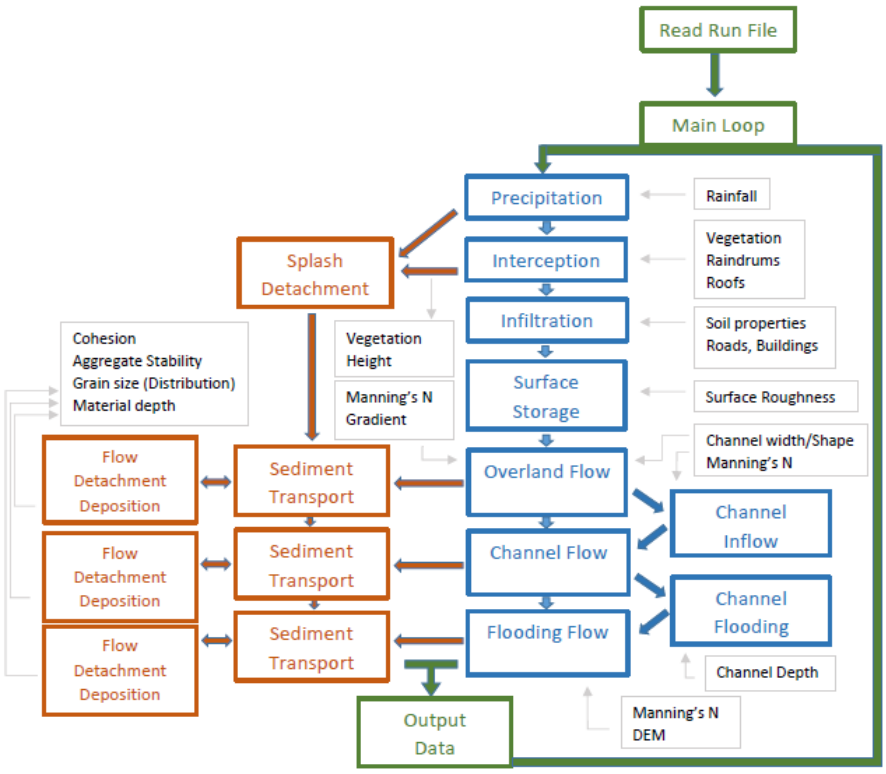

Figure 3: Overview of LISEM workflow, source: Jetten, 2018, p.71

3.2.3 – Initial soil moisture content

The initial soil moisture content (theta-i) is the amount of water in the soil as a fraction between 0 and the porosity. Initial soil moisture can never exceed the porosity and needs to be seen in relation to the porosity. For example, a soil moisture content of 0.3 is not necessarily a small number when the porosity is 0.35. LISEM defines initial soil moisture content as the soil moisture content just prior to a rain shower. The fraction of water that can be stored in the soil is the difference between porosity and initial soil moisture content. Therefore, if the initial soil moisture content is higher, less water of a rain shower is able to infiltrate the soil and more run off. The other way around, lower soil moisture content allows more water to infiltrate and less to runoff.

LISEM works by calculating net precipitation, which is defined as total precipitation minus interception. The second step for the model is calculation of the infiltration rate. This is based on the Darcy relationship equation (Jetten, 2018). The model calculates infiltration using equation 1, which is based on the Green and Ampt method for infiltration.

Equation 1 $$q = -Ksat\left(\frac{d-h}{L} + 1\right)$$

In which $Ksat$ is the saturated hydraulic conductivity in m/s, L is the depth of the wetting front, h the suction at wetting front and d the overpressure depth of the water at soil surface (Baartman et al., 2013). The Green and Ampt method for infiltration is based on the assumption that a wetting front moves downward into the soil parallel to the surface of that soil (Jetten, 2018).

If the Ksat or theta-I values ceteris paribus change, this will lead to another model output in terms of runoff.

3.3 – Time domain reflectometry

Time domain reflectometry (TDR) can be used as an indirect measurement of the soil water content in a soil. It is based on the idea that electromagnetic current travels through a medium – in this case partially wetted soil – with a certain speed. An electromagnetic signal is send between two probes, which are inserted into the ground. The travel time of the signal between these probes can then be calculated using equation 2:

Equation 2 $t = \frac{L}{c}$

In which t is the travel time in seconds, L the signal travel distance in meters and c a constant of $3 * 10^8$ m/s (the speed of electric signal through a vacuum). The velocity of the signal can then be calculated using equation 3:

Equation 3 $v = \frac{L}{t}$

Where v is the speed in metres per second. The dielectric constant of the soil (D), which relates to the soil moisture content, can then be calculated with equation 4:

Equation 4 $D = \left(\frac{c}{v}\right)^2$

3.4 – Accuracy versus precision

The aim of this research is to investigate whether the accuracy of theta-I values can be improved. It is good to give a short description of the concept of accuracy and precision. One could ask why it is important to be as accurate as possible, instead of being as precise as possible. Precision can be described as a way to describe how repeatable a measurement is. A measuring instrument with high precision will give results that are close to each other. This can be compared to shooting arrows at a target, if all arrows hit close to each other, the precision is high. This does not say much of how close the arrows are to the centre of the target however. So, precision is not concerned with how close to the 'target' the measurements are. In other words, measurements that are very precise don't actually have to be close to the true value, the 'target'.

Accuracy on the other hand is a way of indicating how close a value is to the true value. In the example of arrows, it indicates how close to the middle of the target the arrows are. Achieving a high accuracy means that you are close to the real world ('correct') value with your measurements. In this research, the accuracy of data is more important than the precision, because the theta-I values that will be obtained will lead to other model outputs. If they are close to reality (that is, have a high accuracy), model accuracy might also improve.

Accuracy can be difficult to measure. In this research, existing soil moisture sensors will be used which are already calibrated. They can serve as a reliable reference for measurement data from for example the satellite. The data from the sensors can be seen as accurate, so the satellite data should be coming close to these values in order to be accurate.

4 Methods

This chapter provides an overview of all methodology that was used to obtain the results. The first two sections describe the fieldwork that was done and the data that was obtained from Sentinel. Section three details the statistical methods that were used to compare Sentinel and in situ measurements. Sections four to six describe the steps that were taken to model the catchment in LISEM. Lastly, sections seven and eight describe the rainfall events that were used and how they were used to generate LISEM output.

4.1 – Collection of soil moisture data

Soil moisture data were collected using three sources: soil moisture sensors in the soil, Sentinel-based soil moisture maps and manual TDR measurements. The first source, soil moisture sensors, existed of two Campbell CS616 soil moisture sensors at location one and two in figure 4. These sensors were already present due to an ongoing research project and were used to obtain soil moisture data at two depths – 5 and 20 cm. The data from these sensors was saved to a local computer and at were manually transferred to a laptop computer when the locations were visited.

The Sentinel 1 satellite data was used to determine soil moisture levels within the study area. This satellite passes over the catchment roughly once every three days, giving a good temporal frequency. Researchers of the programme Optimizing Water Availability with Sentinel-1 Satellites (OWAS1A) developed an algorithm in which data from the Sentinel-1 satellite can be converted to soil moisture maps using the Google Earth Engine. The base script of this algorithm was obtained from the OWAS1S project (Benninga, van der Velde, & Su, 2016). To be able to calculate the soil moisture value, the soil moisture at wilting point and saturation needed to be incorporated. These data is available for the Netherlands in the form of the *Bodemfysische Eenheidskaart 2012* (BOFEK2012), which is based on the *Staringreeks* (Heinen, Bakker, & Wösten, 2018). Values for soil moisture at wilting point and saturation were obtained from BOFEK2012 (Wösten, Veerman & Stolte, 1994; Wösten et al., 2013). The script that was used can be found in annex 1.

The Sentinel-1 series of soil moisture measurements were converted into graphs for comparison with the Campbell sensor soil moisture series and the manual sampling series. This was done by defining two small areas within the total catchment, one around the location of the northern Campbell sensor (sensor 2) and one around the location of the southern one (sensor 1), see figure 4. For each of these areas, the graph of soil moisture was plotted and compared to the actual Campbell sensor measurements.

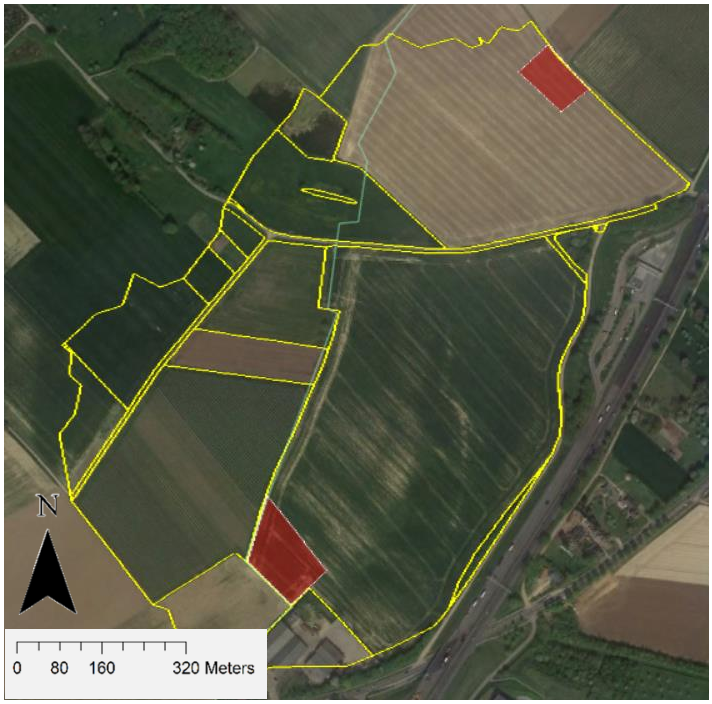

Figure 4: Areas around the two Campbell sensors (red) that were used for Sentinel soil moisture collection. The southern area is location 1, the northern area is location 2.

Next to these soil moisture sensors and satellite observations, manual sampling was conducted to establish the soil moisture content in the soil at a certain day. There are various methods to do this, such as hand sampling and

determining the amount of water in the soil by weighing and drying the soil. The latter takes a lot of time and is not very efficient. Another way to measure this is by using TRD. This is a relatively non-labour intensive and accurate way to measure soil water content. The *HD2 Mobile Moisture Meter* from *Van Walt* was used to perform this part of the fieldwork.

The soil moisture meters provide a reference soil moisture map to the satellite measured soil moisture data. Three fieldwork campaigns were conducted on October 2nd and November 5th ,2019 and March 20th, 2020. The goal was to obtain a soil moisture map on the date of measurement for comparison and evaluation to the data measured by the satellite on the same day. The layout of the November fieldwork can be seen in figure 5. On each sampling point, four subpoints were created in a 10 meter box around the sample location (see annex 2 for more details). The average of all measurements at one location was taken as the soil moisture value at that location.

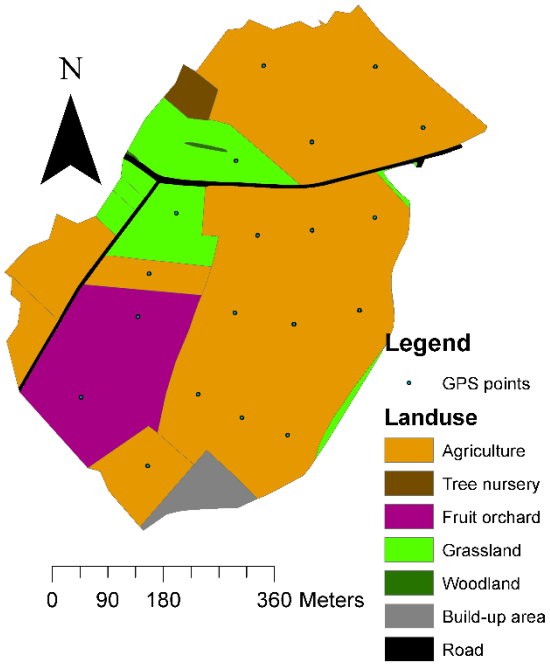

Figure 5: Sampling lay-out November fieldwork

The fruit orchards features two types of land use and according soil moisture and Ksat measurements: within the rows of the trees and between the rows on the grass. These two were distinguished because they likely have very different characteristics in terms of saturated conductivity and soil moisture. So for each location within this orchard one sample was taken withing the tree rows and one in between the tree rows. At the moment of sampling, the apple trees were being harvested.

The March fieldwork featured a slightly different approach. Twenty-three sampling points were selected, per point three measurements were taken. Again, points in the fruit orchard were sampled twice – once in between the trees and once in between the rows. An overview of the sampling points used in the March fieldwork can be seen in figure 6.

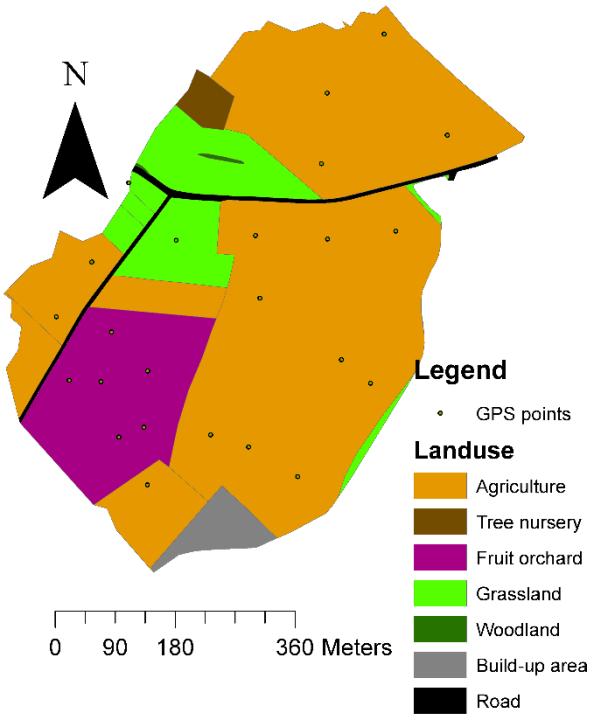

Figure 6: Sampling lay-out March fieldwork

4.2 – Collection and calculation of saturated hydraulic conductivity data

The Ksat measurements were done along the lines of the steps mentioned in the Manual for soil physical measurements. For each measurement, two anchor rods were drilled into the soil, an horizontal rod was placed between them, secured with bolts to prevent movement. The sample ring was equipped with an iron cutting ring to ensure smoother passing into the soil, see figure 7. A hydraulic pump was then used to drill the ring into the soil with minimal soil disturbance (Stolte, 1997). One difference to figure 7 is that these Ksat samples were taken from the topsoil, not the subsoil. After the Ksat samples were taken, they were numbered, rolled in plastic and stored in a cool room to be analysed.

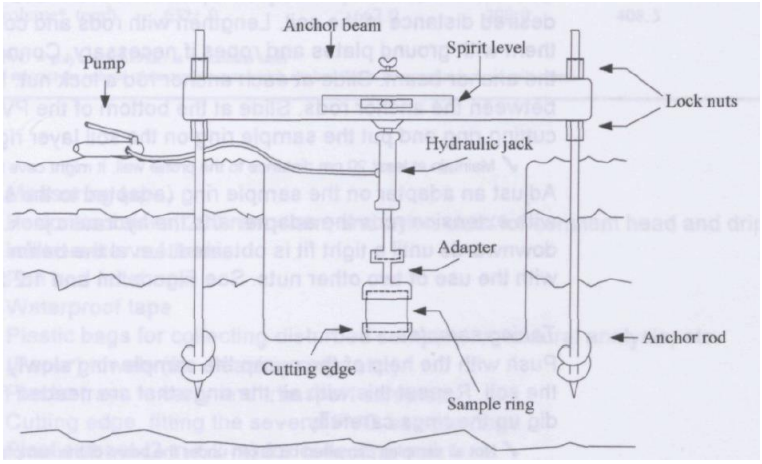

Figure 7: Hydraulic conductivity measurement method. Source: Stolte, 1997, page 14

Analysis of the Ksat samples was done using the *Standaardwerkvoorschrift bepaling van de verzadigde waterdoorlatendheid*, which is based on the NEN5789 protocol. The samples were carefully trimmed so that they exactly matched the top and bottom extend of the ring. They were then placed in a layer of a few centimetres of water to slowly start infiltration. After a week they were put in the measurement setup. Once the whole sample was saturated and a small layer of water appeared on top of the sample, a column of approximately ten centimetres of water was put on top of the sample and twenty-four hours later, the measurement of hydraulic conductivity was carried out, an example of the setup used can be seen in figure 8. For each sample, three measurements of Ksat were taken with each measurement lasting at least ten minutes and collecting at least 100 millilitres of water, in accordance with the aforementioned protocol.

Figure 8: Measurement setup during measurements of Ksat samples

The Ksat values were calculated according to the equations 5 and 6:

Equation 5 $$Ksat = \frac{V}{|\Delta H| * \Delta t * A}$$

In which in *equation 6* $|\Delta H| = \frac{z_{top} - z_{out}}{L}$ and $q = \frac{V}{\Delta t * A}$

In which V is the volume of water that was collected in Δt time, L the height of the sample and A the area of the sample.

4.3 – Comparison of Sentinel and measured data

The Google Earth engine was used to create a graph of average VWC in the total catchment and in the locations of the Campbell sensors during the year 2019. The VWC values measured with these sensors were averaged per day and put in a graph as well. Direct comparison of these graphs was difficult, so a statistical approach was used to determine the correlation *r* between the Sentinel daily averages on locations of the Campbell sensors and the daily averages measures by these sensors. This was done by calculating the Pearson correlation coefficient *r* with equation 7:

Equation 7 $$r = \frac{1}{n-1}\left(\frac{\sum(x-E(x))*\sum(y-E(y))}{s_x*s_y}\right)$$

in which *E(x), E(y)* are the average values of the x and y variable, *n* is the number of data points that *x* and *y* share and *s(x), s(y)* are the standard deviations of the variables. The standard deviations *s* were calculated using equation 8:

Equation 8 $$s = \sqrt{\frac{\sum(x-E(x))^2}{n-1}}$$

in which *E(x)* is the average value of the *x* variable and *n* is the number of values over which the standard deviation is calculated.

Another way that the Sentinel data were compared to the data measured with the Campbell sensors is by using the RMSE. The Sentinel based values were determined 'model' outputs, the Campbell sensor data the 'observed' date. Equation 9 was used:

Equation 9 $$RMSE = \sqrt{\frac{\sum(x_{modeled}-x_{observed})\text{^}2}{n}}$$

In which *n* is the number of observation pairs and, $x_{modeled}$ are the Sentinel SWC values and $x_{observed}$ are the Campbell sensor SWX values.

The third way that the Sentinel and soil moisture sensor data were compared was by using the Nash Sutcliffe coefficient (NSE). The NSE was calculated using equation 10:

Equation 10 $$NSE = 1 - \frac{\sum_{t=1}^{T}(Q_o^t-Q_m^t)\text{^}2}{\sum_{t=1}^{T}(Q_o^t-\overline{Q_o})\text{^}2}$$

In which Q_o^t are the observed values – in this case the VWC values observed with the soil moisture sensors – Q_m^t are the modelled values – in this case the VWC measured with Sentinel.

4.4 – Data processing and setting up LISEM

Preparation of data for LISEM was done using the Nutshell software – which is a Windows shell for PCraster, the input map type that is required for LISEM. A PCraster script was used to create all needed maps for LISEM to run. This script can be found in annex 3.

The soil moisture maps that Sentinel provides are ten meter resolution and cover the whole catchment. In LISEM, one soil moisture per field was assigned. Therefore, the Sentinel picture needed to be broken down into field-size parts. This was done with the *Arcmap* software and is visualised in figure 9.

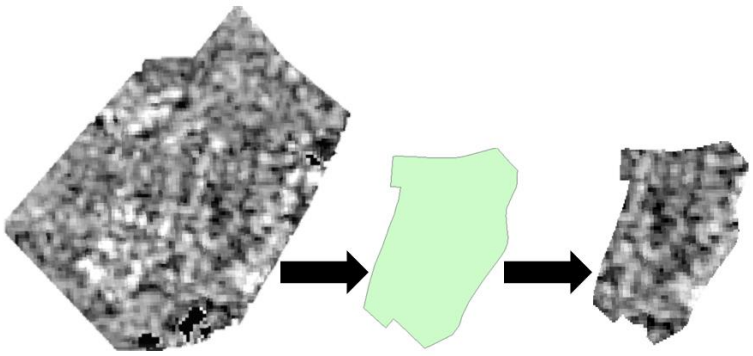

Figure 92: Out of the Sentinel images, smaller portions the size of individual fields were cut

Every field was made into a separate feature. A Sentinel image was then used out of which all fields were clipped. The result being Sentinel images per field in the catchment. These individual files were used to find the average soil moisture value, which were then used as input for LISEM. Table 2 provides an example of all data that were used per field of the study area. In the different runs and scenario's, values of this table were adjusted. A short explanation of each of the parameters will be given now.

Land use: see table 2 for land use corresponding to the field numbers. Numbers 90, 91 and 100 are roads or build-up area.

Random roughness, **Manning's N, LAI and PSI** were chosen based on appendix A and B of the LISEM manual, which provides values for these variables based on their land use (Jetten, 2018).

Porosity: the soil samples that were used to determine Ksat were afterwards used to determine porosity. They were weighed when completely saturated, then dried in an 105 degrees Celsius oven for 72 hours and weighed again. To determine porosity, equation 11 was used for this:

Equation 11 $$Porosity = \frac{W_{wet} - W_{dry}}{V} * 100$$

In which W_{wet} is the wet weight, W_{dry} the dry weight, both in kg, and V the volume in m^3. This was done for ten samples. The average porosity was calculated to be 44.5. This value was used for the entire catchment.

Hydraulic conductivity: the calculated Ksat based on samples was averaged per field, outliers were excluded. To see whether measured values provide results closer to observed in the catchment, Ksat values for LISEM run without measured Ksat values were taken from appendix A of the LISEM manual.

Initial soil moisture content this value changes depending on the day the model was run at. This field was used in two ways. Either it contains the average Sentinel-1 value of soil moisture for a field on a certain day or it contains the average sampled value per field for a certain day.

Soil depth was set to ten centimetres for the whole catchment. It influences the infiltration potential, as deeper soils can retain more water than shallower soils. The value of ten centimetres is a rough estimation. Soil in Limburg are deeper but deeper soil do not have a significant impact on the runoff of LISEM.

Table 2: Example of table that was used as LISEM input

Field #	Landuse	Random roughness	Manning's N	Stone fraction	Cohesion	Aggregate stability	D50	Ksat	PSI	Porosity	Initial soil moisture	Soil depth	PER	LAI	CH	Additional cohesion
1	Cropland	1	0.03	0	15	15	40	40.8	15	0.45	0.15	100	1	1.7	0.4	0
2	Cropland	0	0	0	15	15	40	40.8	15	0.45	0.27	100	1	1.7	0.4	0
3	Grassland	0.5	0.1	0	15	15	40	124	15	0.45	0.28	100	1	6	0.2	0
4	Fruit orchard	1	0.1	0	15	15	40	828	15	0.45	0.29	100	1	1	3	0
5	Cropland	1	0.1	0	15	15	40	40.8	15	0.45	0.16	100	1	1.7	0.4	0
6	Cropland	1	0.1	0	15	15	40	40.8	15	0.45	0.26	100	1	1.7	0.4	0
7	Cropland	1	0.1	0	15	15	40	40.8	15	0.45	0.29	100	1	1.7	0.4	0
8	Cropland	1	0.03	0	15	15	40	40.8	15	0.45	0.36	100	1	1.7	0.4	0
9	Grassland	1	0.03	0	15	15	40	124	15	0.45	0.27	100	1	1.7	0.4	0
10	Grassland	0.5	0.1	0	15	15	40	124	15	0.45	0.3	100	1	6	0.2	0
11	Tree nursery	1	0.1	0	15	15	40	828	15	0.45	0.28	100	1	1	3	0
12	Grassland	0.5	0.1	0	15	15	40	124	15	0.45	0.32	100	1	6	0.2	0
13	Grassland	0.5	0.1	0	15	15	40	124	15	0.45	0.35	100	1	6	0.2	0
60	Woodland	1	0.1	0	15	15	40	124	15	0.45	0.25	100	1	6	0.2	0
60	Woodland	1	0.1	0	15	15	40	124	15	0.45	0.3	100	1	6	0.2	0
70	Grassland	0.5	0.1	0	15	15	40	124	15	0.45	0.25	100	1	6	0.2	0
70	Grassland	0.5	0.1	0	15	15	40	124	15	0.45	0.23	100	1	6	0.2	0
90	Road	0	0	0	15	15	40	0	15	0.45	0	0	1	0	0	0
91	Road	0	0	0	15	15	40	0	15	0.45	0	0	1	0	0	0
100	Build-up area	1	0.01	0	15	15	40	1000	15	0.45	0	100	1	0	0	0

4.5 – Modelling ridges

The objective of a model is to resemble the real word as accurately as possible. Complete accuracy is really difficult and hard to achieve in a study like this since there are endless ways to make a model more accurate. The opposite of this is a model that is too simple and overlooks major aspects of the process or catchment. An important feature that influences runoff a lot is the presence of potato ridges during growing season on the main agricultural field.

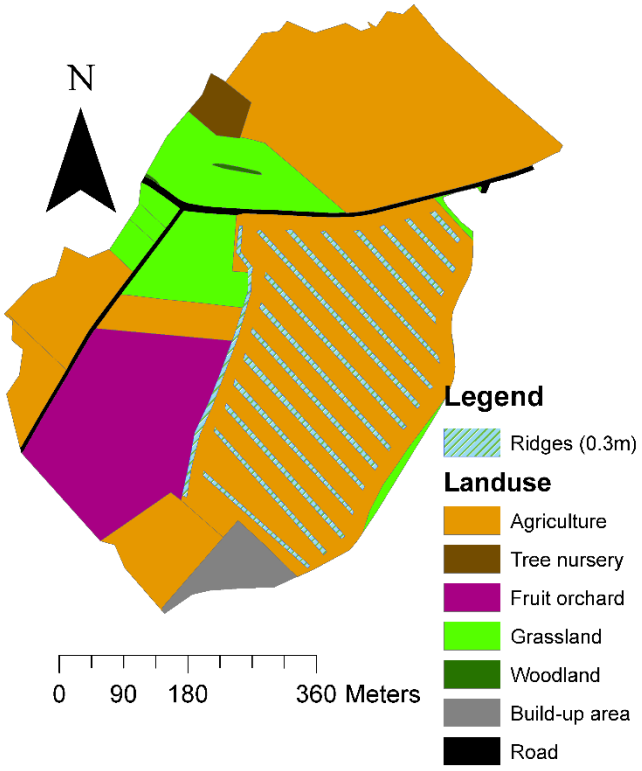

Figure 10: Modelled ridges

LISEM makes use of DEM. The DEM that was used in LISEM – as well as all other data – had a resolution of 5 metres. Each cell within the DEM contains a value for its height above sea level. A way to build barriers is to build them into the DEM. This was done by creating features in Arcmap with the same direction as ridges, a z-value of 0.3 was assigned to each feature. Observations in the Catsop catchment shows ridges following contour lines on the western part of field number 2. These ridges rapidly guide the water down to the outlet. To model this in LISEM, one ridge was added in the same direction and with the same function as these ridges. A complete overview of the ridges can be seen in figure 10.

All area that was no ridge was given value 0. This file was converted to ASCII file format. Nutshell was used to convert the ASCII to a .map file and add the z-value of the features to the DEM. This was done using the following two commands:

$$asc2map - a\ barriers.asc\ barriers.map - -clone\ clone.map$$

$$pcrcalc\ dem2.map = dem.map + barriers.map$$

This results in a DEM in which the ridges are modelled with cells that are 0.3 meters higher than the surrounding area. The resulting a non-edited DEM and a DEM with barriers can be seen in figure 11. This is a solution that allows modelling of ridges, however it is far from an ideal solution. Since the cell size of the DEM is five meters, the modelled ridges are immense (5 by 5 by 0.3 meters) compared to ridges one would see in a field. These modelled ridges do have a similar effect as normal ridges, namely to act as water barriers. The LISEM run with

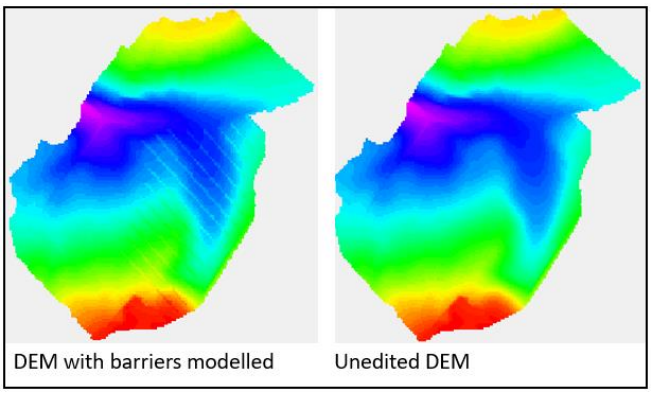

Figure 41: Normal DEM and modified DEM to simulate potato ridges

barriers provides flow patterns that look more close to observed patterns than the LISEM run without barriers.

4.6 – Selection of rainfall events

Three of these rainstorms for which LISEM runs were done were selected. The rainfall data itself were obtained from ongoing, unpublished, research in the Catsop area. The nature of the required storms has been discussed earlier: they need to be relatively short and relatively intensive so that they actually produce measurable runoff. Another criterium that was taken into account is the availability of soil moisture data on or around the date of the storm. Table 3 lists the three storms that were selected based on this criterium.

Table 3: Selected rain storms and their characteristics

Date	Total rainfall (mm)	Max. intensity in 5 minute window (mm/h)	Duration (hours)	Qmax (L/sec)
March 15th, 2019	24.2	28.8	4:00	140
May 28th, 2019	5.4	19.2	1:08	284
September 29th, 2019	4.2	33.6	0:31	104

4.7 – Rainfall and runoff selection, calculations and comparisons

A summary of the workflow to get LISEM working for the three rainfall events can be seen in figure 13. For all three rainstorms, the same data on cohesion, aggregate stability etc. were used. The hydraulic conductivity map from figure 23 (see chapter 6) was used for the first run, the literature based hydraulic conductivity values (see section 5.6) were used during the second run. Individual soil moisture maps were created for each of the three rain storms, these maps are displayed in figure 24 (chapter 6). Unique rainfall files, that can be found in annex 4 were used for each rain shower. The LISEM model was then calibrated to match the recorded runoff of the rain storm as measured by the water board. The two parameters in LISEM that were used to calibrate were the *multiplication factor Ksat slopes* and *multiplication factor Manning N slopes*. The discharge LISEM using the measured hydraulic conductivity values and the theory-based hydraulic conductivity values were combined in graphs with the discharge measured by the water board, see figure 25 (chapter 6).

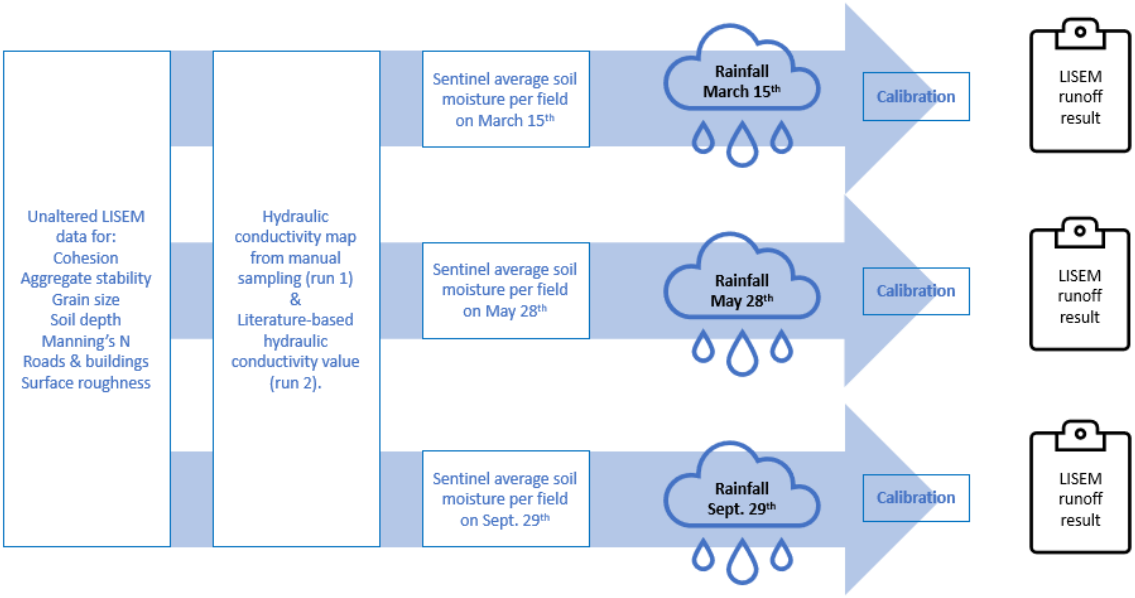

Figure 53: Schematic of LISEM data workflow for the three selected rain showers

4.8 – Calibration

OpenLisem offers a few calibration parameters, of which the Ksat and Manning's N are the most sensitive (De Roo & Jetten, 1999; De Roo, Offermans & Cremers, 1996). The main focus of the calibration was to match the peak discharge and the speed at which the outflow decreases after the peak discharge.

5 Results

5.1 – Soil moisture data from fieldwork, Sentinel and Campbell sensors

Soil moisture data from three sources is available. Both the Sentinel and Campbell sensors can provide continuous information. The soil sampling provides data on a few specific dates. The average soil moisture data in the area as captured by the Sentinel-1 satellite during the year 2019 is shown in figure 15. In figures 16 and 17 the mean soil moisture values in the areas surrounding the Campbell sensors is plotted for the year 2019. As can be seen from figure 14 and 15, the VWC is quite high throughout the whole year, but is lower during the start of the growing season (April – June).

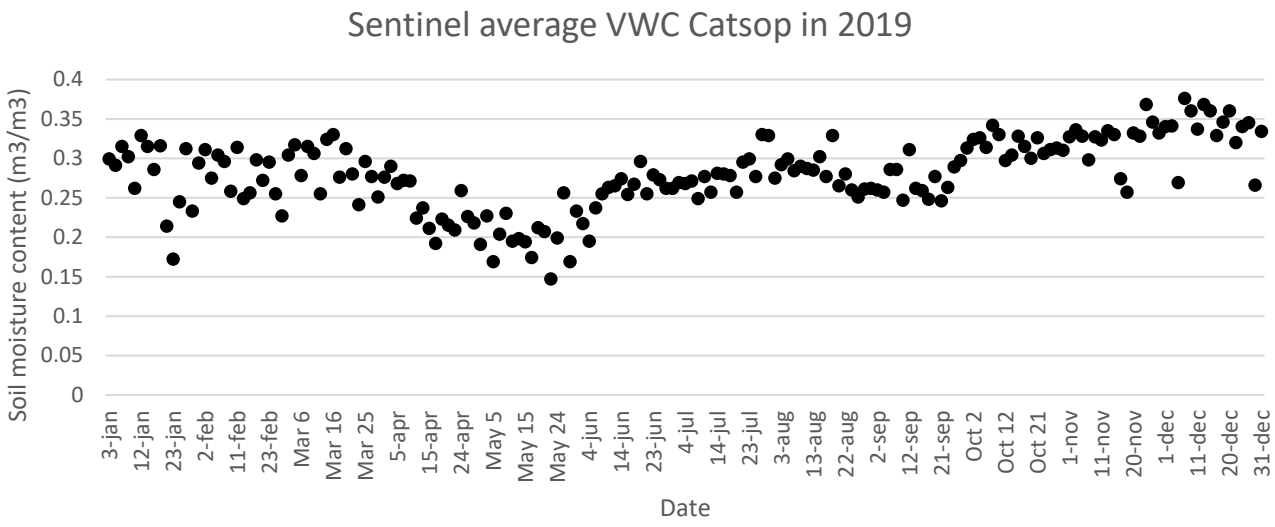

Figure 64: Sentinel average VWC Catsop 2019

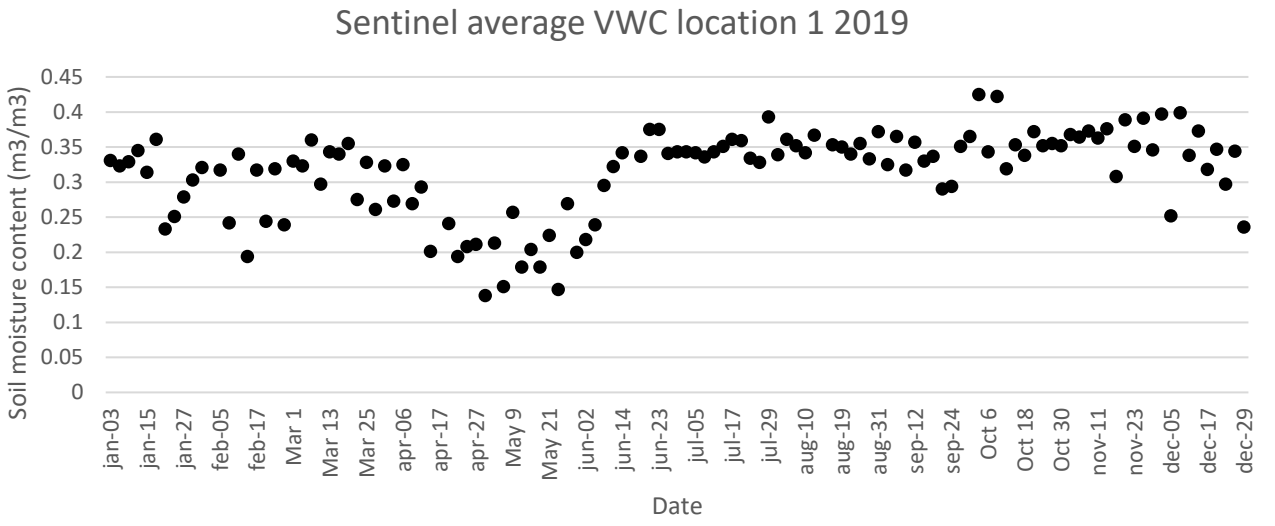

Figure 15: Sentinel average VWC at location 1 in 2019

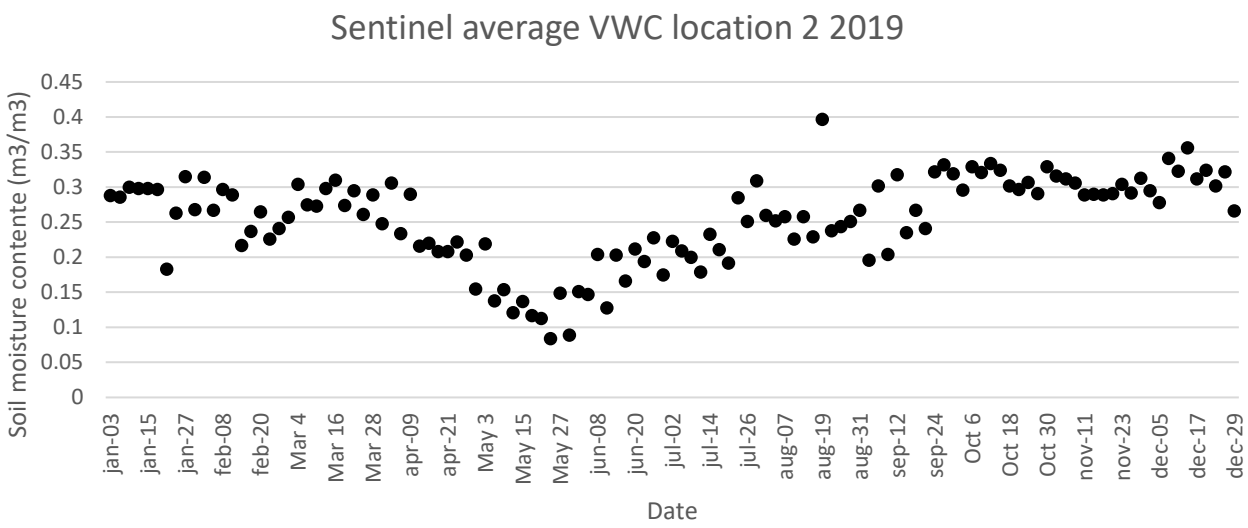

Figure 16: Sentinel average VWC location 2 in 2019

Based on the automatic observations of the Campbell sensors it is also possible to plot a graph of the measured SWC during 2019, see figure 17 and 19. These graphs show the daily average soil moisture at 5 and 20 cm depth. The data are averages per day and days or periods with no data were removed.

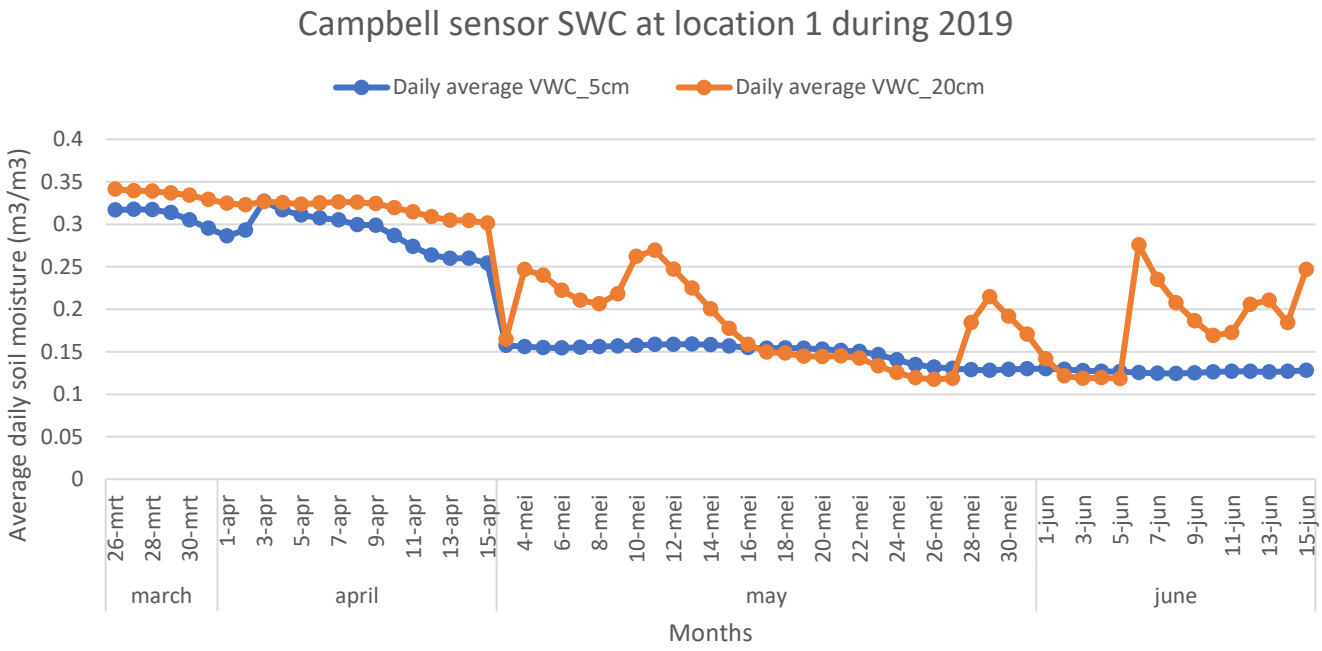

Figure 17: Campbell sensor SWC at location 1 in 2019

When data from the Campbell sensors at locations 1 and the Sentinel averages for location 1 and 2 are combined, the result can be displayed in figure 18 and 20. These are again daily averages. As can be seen in figure 17, location one has little days where both Sentinel and Campbell contain measurements. Both Campbell and Sentinel seem to follow the same trend. In figure 20 some larger differences between Sentinel and Campbell can be seen, especially as the growing season progresses.

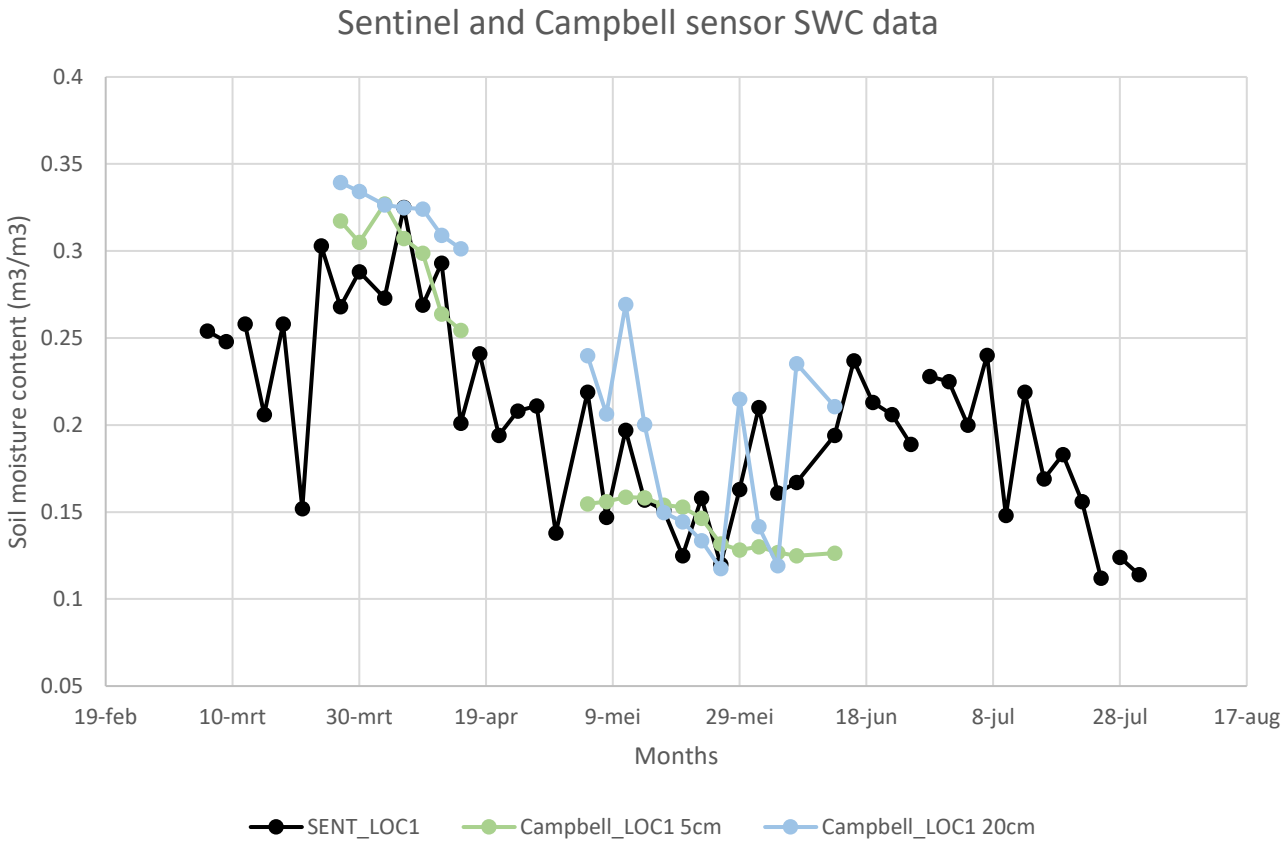

Figure 18: Combined Sentinel and Campbell SWC at location 1

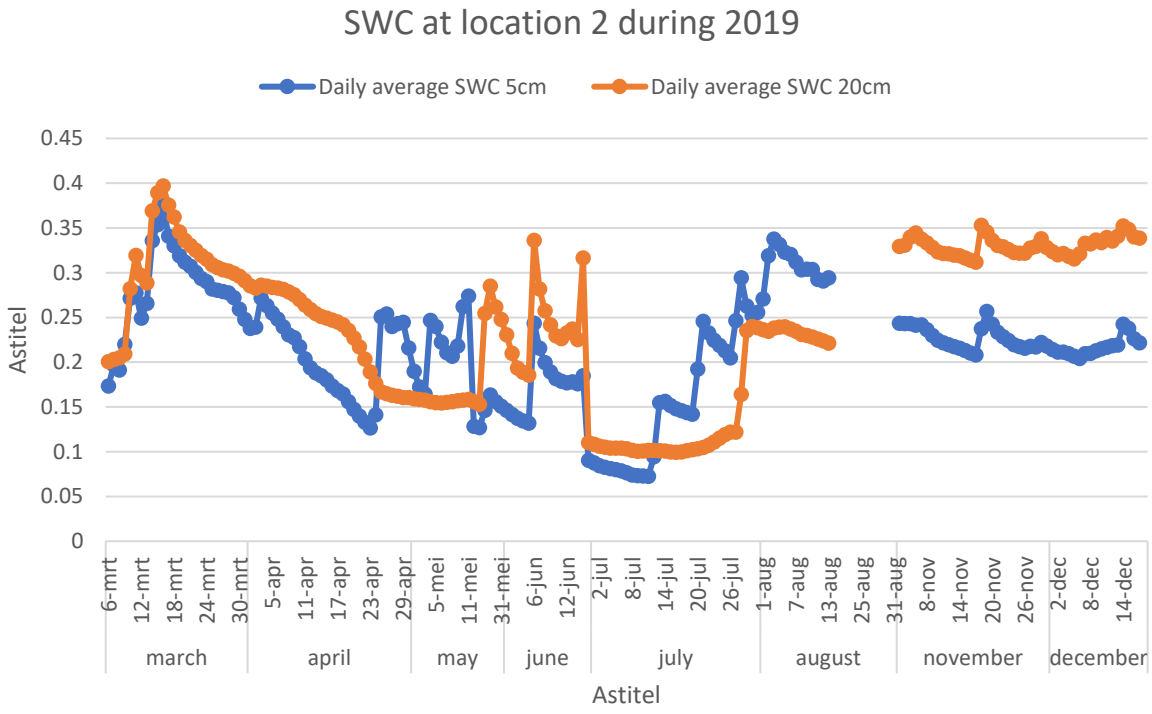

Figure 19:Campbell sensor SWC at location 1 in 2019

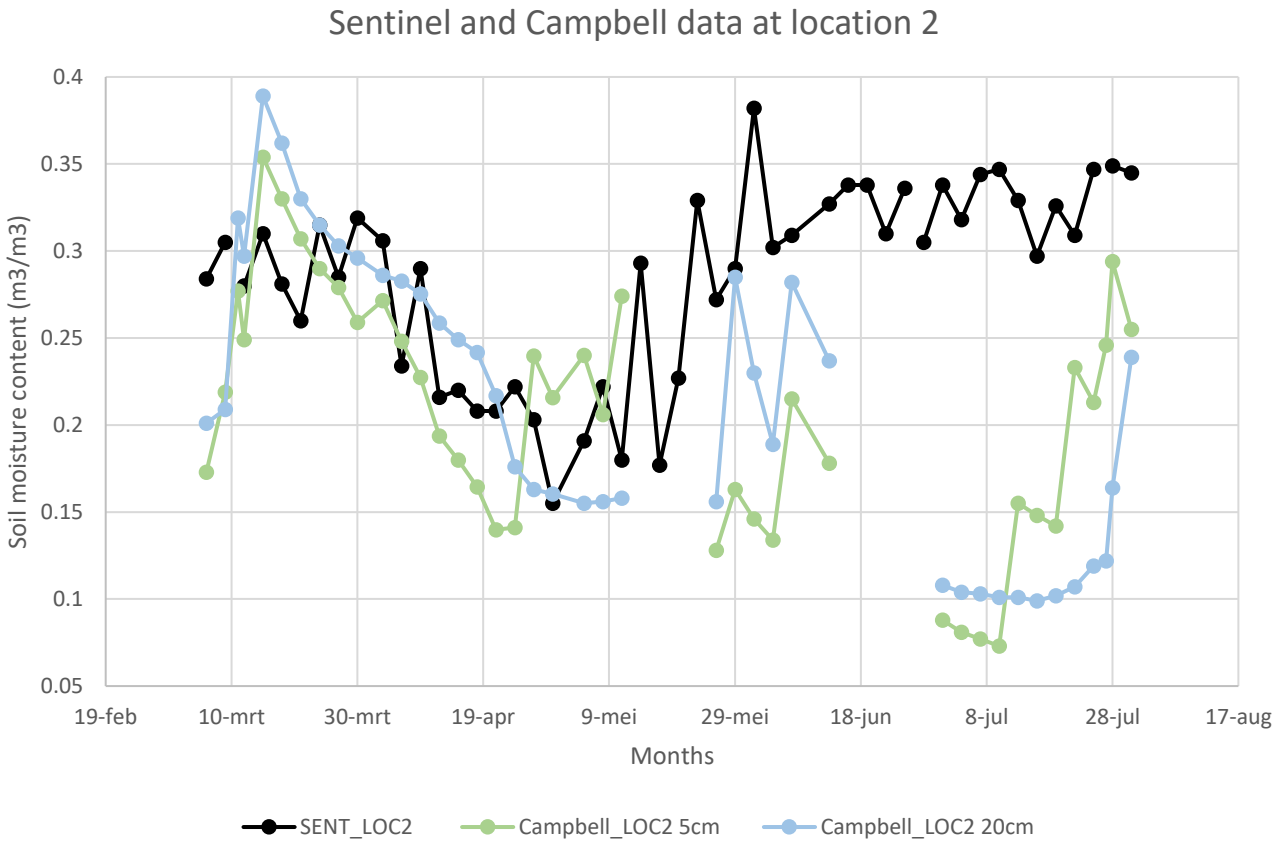

Figure 20: Combined Sentinel and Campbell SWC at location 2

Based on these graphs the correlation *r* and r^2 between Sentinel and Campbell sensors were calculated. The Sentinel data of location 1 were coupled to the 5cm and 20cm Campbell sensor data of location 1. The same was done for location 2. The results can be seen in figure 21.

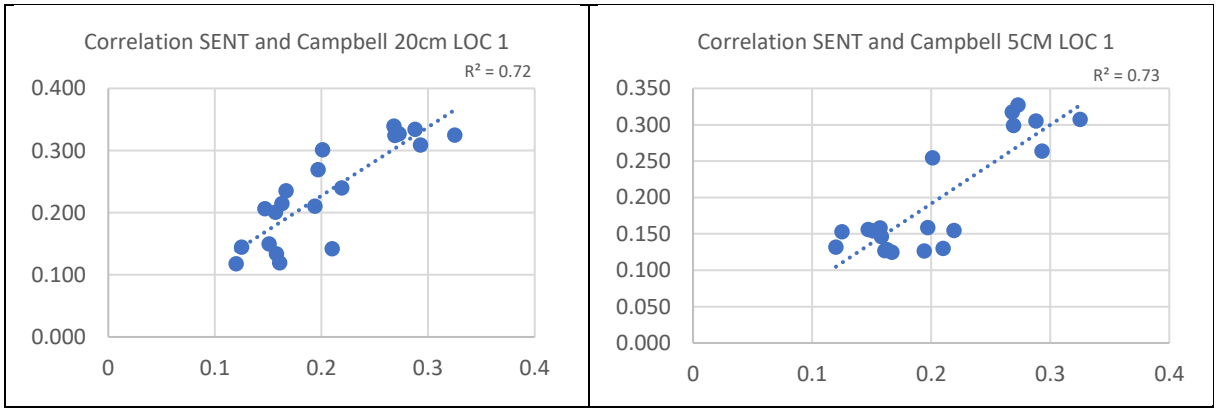

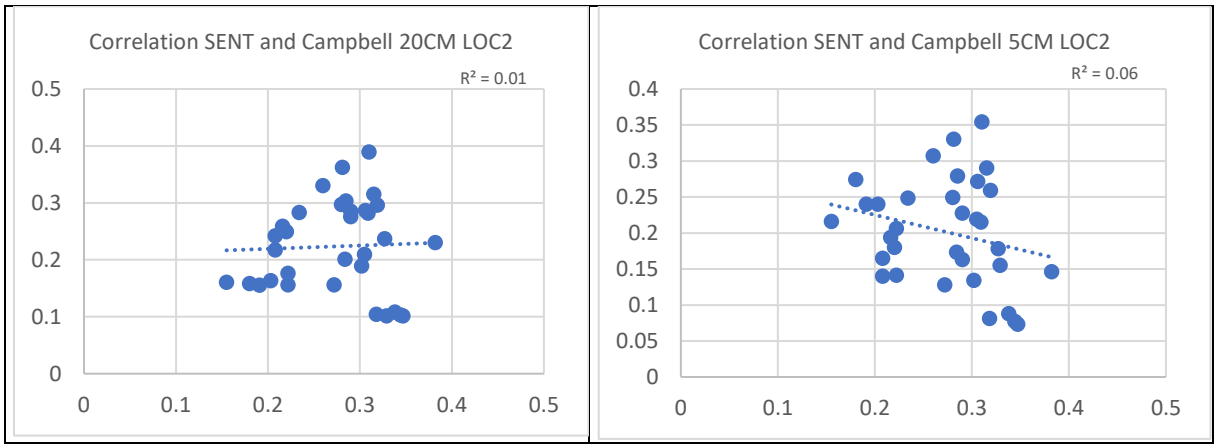

Figure 7: Correlation of VWC between Sentinel and Campbell sensors at Location 1 (upper graphs) and location 2 (lower graphs). Outliers not yet excluded.

From these results it is clear that no relationship can be found between the location 2 Sentinel and Campbell sensors data. Both $r = 0.04$ and $r = 0.2449$ are low values indicating no significant relationship between the two. The Sentinel images of location 1 and the values of the Campbell sensors seem to better correlate with r values of 0.86 and 0.85 for 5 and 20 cm Campbell sensors respectively.

Using the Sentinel data as modelled output and the soil sensor measurements as observed output, it is possible to calculate the Nash Sutcliffe coefficient. In table 4, the NSE for Sentinel 1 data compared to in-field soil moisture measurements can be seen.

Table 4: Nash Sutcliffe coefficient and RMSE for Sentinel and observed soil moisture data

Modelled data	**Sentinel loc1**	**Sentinel loc1**	**Sentinel loc2**	**Sentinel loc2**
Observed data	**Campbell loc1 5cm**	**Campbell loc1 20cm**	**Campbell loc2 5cm**	**Campbell loc2 20cm**
NSE	0.89	0.85	-0.16	0.21
RMSE	0.04	0.05	0.14	0.13

These results indicate a moderately good match between the Sentinel and observed data at location 1. The negative values for location two indicate that Sentinel data is not as good as observed data.

In order to compare the satellite imagery with measured values, another possibility is to look at the fieldwork soil moisture values per field and compare them to the Sentinel average values for the same field on the same day. Unfortunately, there are no Sentinel data on the exact dates of fieldwork since not every day or even every pass-by of Sentinel produces a usable image. table 5 gives an overview of the available Sentinel data and precipitation around the fieldwork data (the thick-boxed dates)

Table 5: Rainfall and Sentinel data availability. Source: KNMI, station Beek

Date	Rainfall (mm)*	Sentinel-image
OCTOBER FIELDWORK		
1-10-19	7.2	NO
2-10-19	19.3	YES
3-10-19	7.2	NO
NOVEMBER FIELDWORK		
4-11-19	2.8	NO
5-11-19	3.3	NO
6-11-19	3.4	NO
7-11-19	1.2	YES
8-11-19	2.1	NO
MARCH FIELDWORK		
28-02-20	13.90	NO
29-02-20	3.90	NO
1-03-20	2.70	YES
2-03-20	2.50	NO
3-03-20	7.90	NO
4-03-20	0.40	NO
5-03-20	1.30	NO
6-03-20	16.40	NO
7-03-20	4.00	YES
***Source: KNMI, station Beek**		

As mentioned before, the Sentinel passes over the study area every three days. The only direct match with a fieldwork date is October 2nd, 2019. The large amount of time between satellite passing and fieldwork, and the rain that fell in that time makes comparing the collected soil moisture data from the November and March fieldwork impossible. Table 6 gives the comparison between the Sentinel and measured SWC values in October, November and March.

Table 6: Comparison between measured and Sentinel soil moisture content

#	Land use	NOV_FW*	NOV_SENT*	OCT_SENT	OCT_FW	MAR_SENT	MAR_FW
1	Cropland	34	29	41	21	32	38
2	Cropland	32	36	36	17	32	35
3	Grassland	40	25	29	21	32	50
4	Fruit orchard	33	29	26	25	36	39
5	Cropland	31	31	31	18	34	35
6	Cropland	31	37	37	20	32	N/A
7	Cropland	31	34	25	22	31	32
8	Cropland	35	31	33	22	31	N/A
9	Grassland	35	28	32	26	35	N/A
10	Grassland	40	31	25	25	31	61
11	Tree nursery	33	28	31	25	32	N/A
12	Grasland	40	25	24	24	33	N/A
13	Grassland	40	31	29	24	31	N/A
60	Woodland	40	25	20	24	34	N/A

60	Woodland	40	28	30	24	38	N/A
70	Grassland	40	33	30	24	39	N/A
70	Grassland	40	32	33	24	31	N/A

*FW means fieldwork data, SENT means Sentinel data

Since there are several days with precipitation between the November and March fieldwork and Sentinel passes, the only date on which Sentinel soil moisture values can be compared to sampled values is October 2nd, 2019. The result of this comparison can be seen in figure 22.

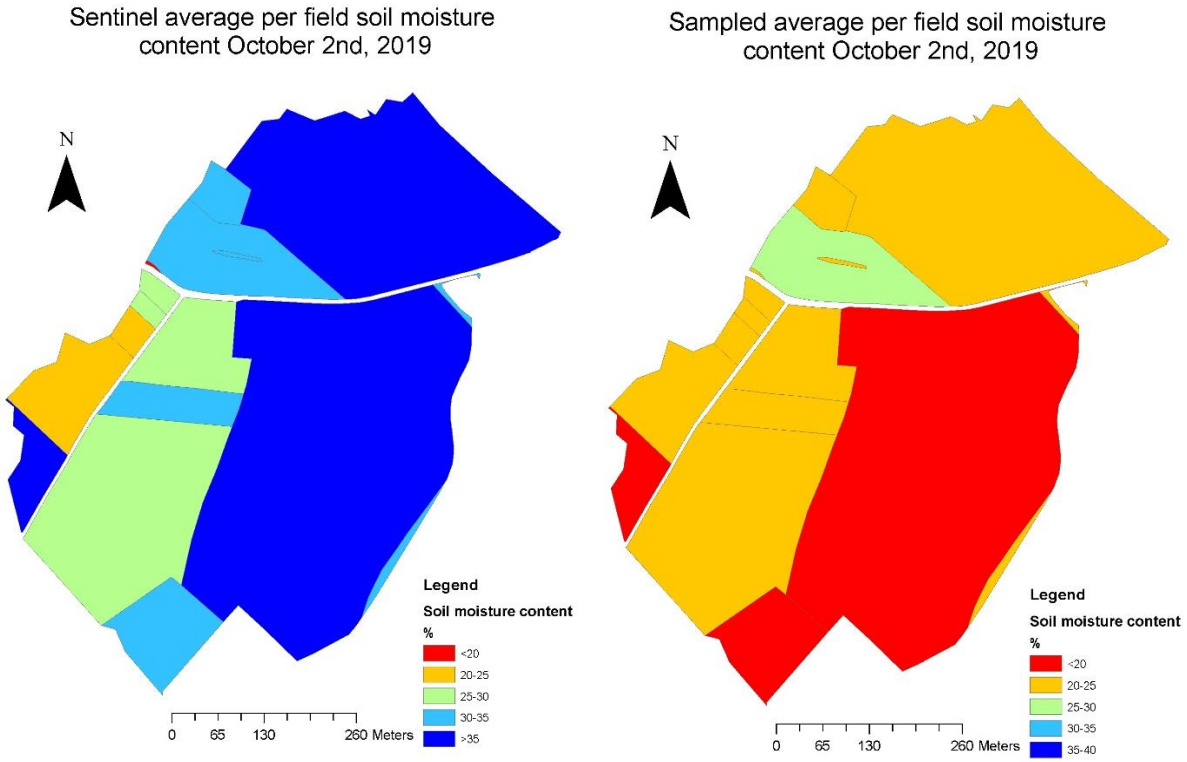

Figure 22: Comparison of average soil moisture per field from manual sampling and Sentinel

5.2 – Soil moisture and hydraulic conductivity maps

5.2.1 – Literature-based hydraulic conductivity values

One of the goals of this paper is to compare measured hydraulic conductivity to values of that same variable that would otherwise be obtained from other sources. In other words: what would a literature-based hydraulic conductivity value for this catchment be and does it produce different results compared to the measured values.

Since hydraulic conductivity depends on the type of soil, the first step is to find the soil type in the catchment. Using the *Bodemfysische Eenheidskaart* from 2012, the soil type in the catchment was defined as silty loam (Wösten, et al., 2013). In the *Staringreeks*, this is called soil type B14 (silty loam) with a hydraulic conductivity value of 0.9 cm/day (fitted, not measured). However, from all the B14 sampling locations in this *Staringreeks*, there is a large difference in hydraulic conductivity ranging between 0.02 to 99 cm/day. Even on sampled locations that are labelled with the same coordinates, large differences in hydraulic conductivity occur (Heinen, Bakker, & Wösten, 2018). Other research found hydraulic conductivity values for the B14 soil type to be 34.5 and 133.5 cm/day. The locations of measurements I this research are – unfortunately – not documented. (Bakker, Heinen, de Groot, Assinck, & Hummelink, 2018). The problem of hydraulic conductivity values being not well documented is already described in older studies as well, these studies established a hydraulic conductivity of 1mm/hour for farmland and 3mm/h grasslands (Smith, Goodrich, & Unkrich, 1999; De

Roo & Jetten, 1999). Since this last study was in the same catchment and the values of 1 and 3mm respectively fall within mentioned values of the *Staringreeks* and *Bodemfysische Eenheidskaart*, these values were used for the Catsop catchment for comparison against the measured hydraulic conductivity.

5.2.2 – Hydraulic conductivity based on sampling

Based on the Ksat measurements, a map for the Ksat per field (averaged when more than one sample per field was taken) was made, see figure 23. As can be seen, the highest values were found in the fruit orchard and grass fields. The lower values were found on land used for agriculture. The black piece of land is a farm that has a paved compound

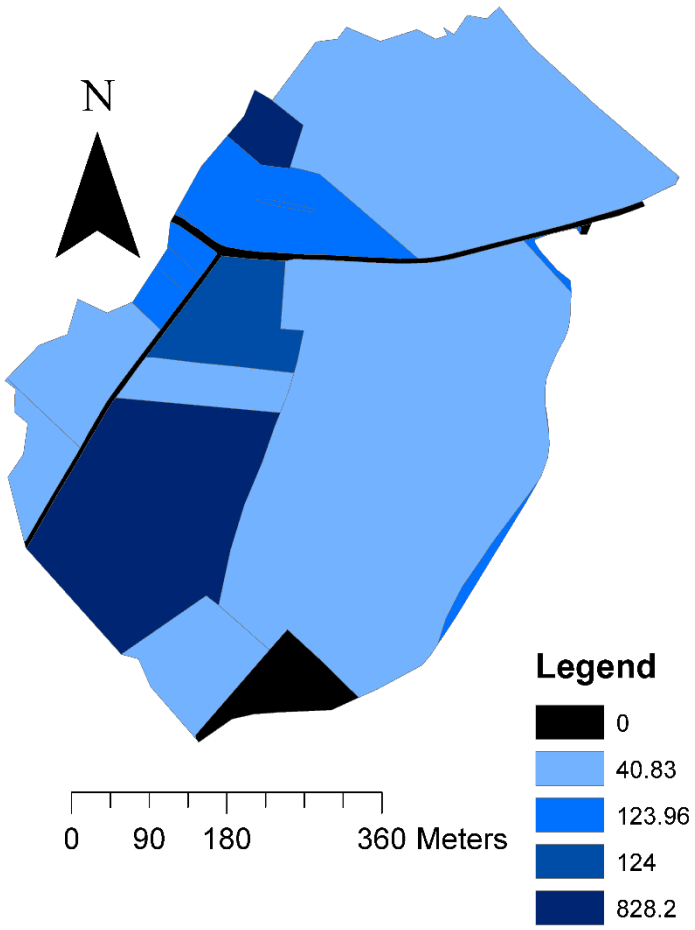

Figure 8: Hydraulic conductivity (mm/hour)

5.3 – LISEM run results for three rain storms

As mentioned in the methods chapter, three rain storms were used for the LISEM modelling. For each of these storms, a theta-I map based on Sentinel data was created containing average soil moisture values per field on the day before the storm, the soil average soil moisture per field is displayed as a percentage of the porosity (0.445). The resulting maps can be seen in figure 24 on the next page.

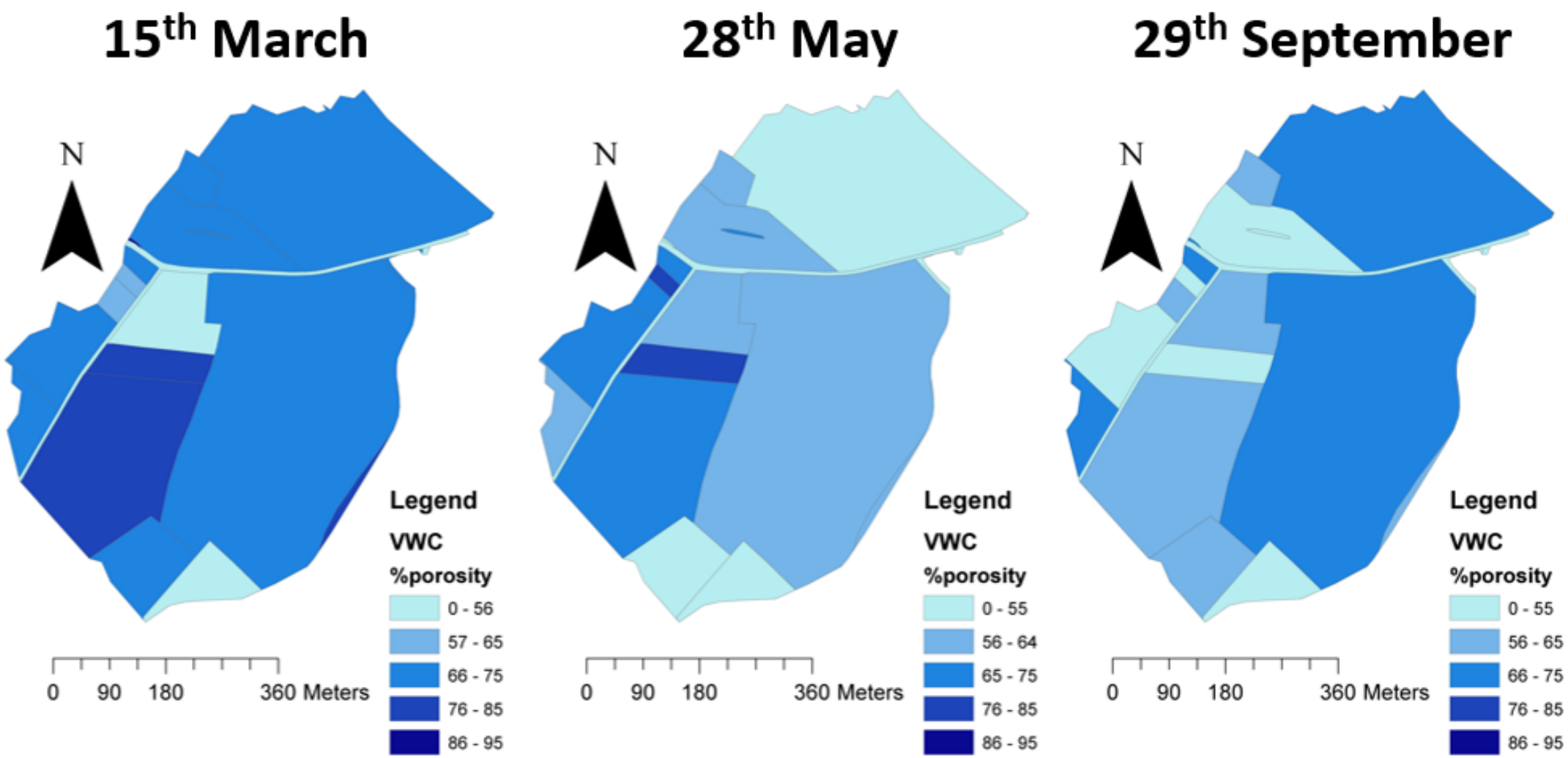

Figure 24: Average Volumetric Water Content obtained from Sentinel per field for the three selected rain showers

The LISEM calibration settings and the Ksat ranges that were used for the three rainfall events can be seen in table 7. The ranges for Ksat values are given, the exact values for manual sampled runs can be found in figure 23. The literature based Ksat values can be found in section 5.2.1 The hydrographs of the three rainfall events can be found in figure 25. The absolute values of Manning's N were not changed for each of the runs. They have a range between 0.001 for the agricultural fields and grassland and 0.1 for the fruit orchard. Manning's N for roads was set as low as possible.

Table 7: Comparison of LISEM settings for manual and literature based Ksat samples

	March 15th	May 28th	September 29th
Manually sampled Ksat values (run 1, for exact Ksat values)			
Ksat range [min,max] (mm/h)	[40.83, 828.2]	[40.83, 828.2]	[40.83, 828.2]
Ksat calibration factor (-)	0.04	0.01	0.03
Manning's N calibration factor (-)	0.50	0.01	0.01
Litarature based Ksat values (run 2)			
Ksat range [min, max] (mm/h)	[1, 3]	[1, 3]	[1, 3]
Ksat calibration factor (-)	1.60	0.40	1.20
Manning's N calibration factor (-)	0.50	0.01	0.01

As can be seen in figure 25, the LISEM runs mostly result in less total runoff than measured in the field. For the showers in May and September using the literature Ksat values, it is possible to better approximate observed values.

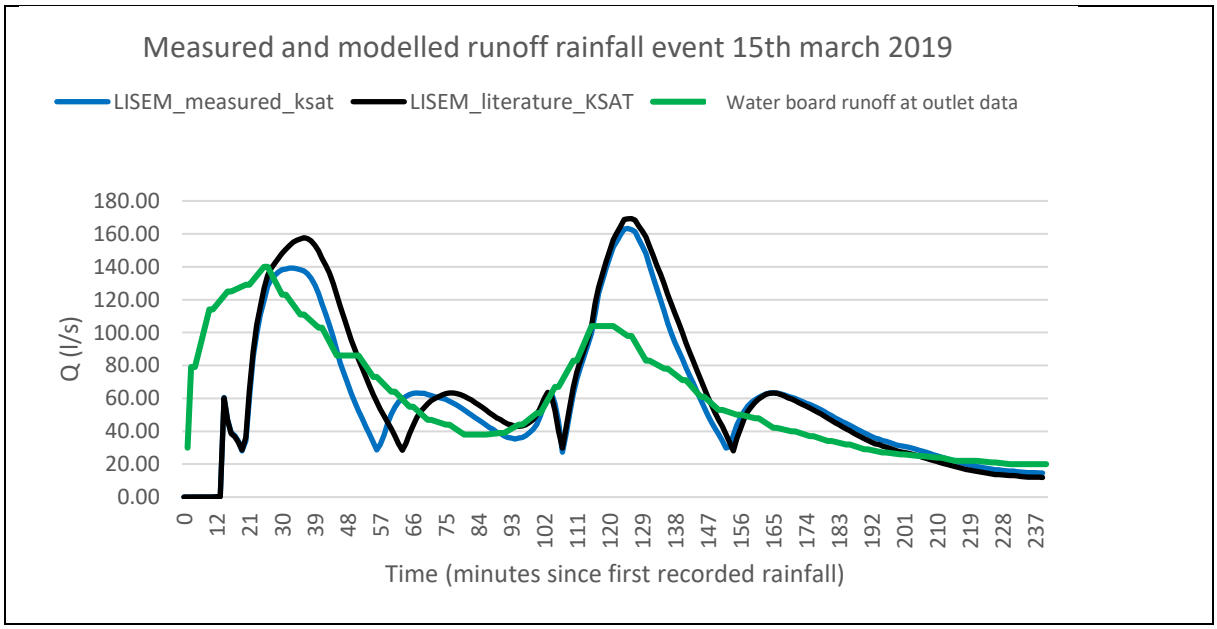

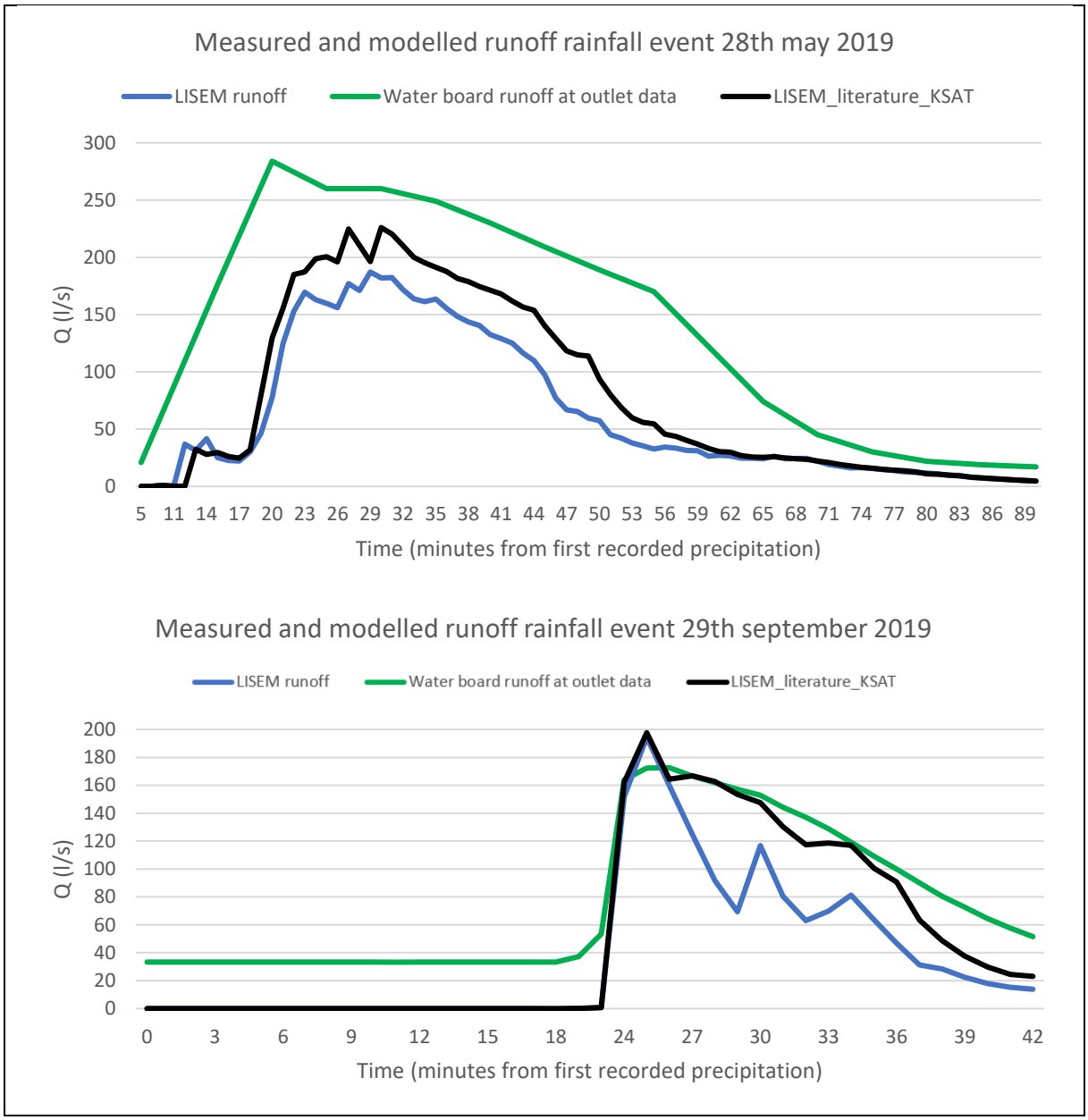

Figure 9: Comparison of hydrographs for three rainfall events

6 Discussion

This research showed that it is possible to compare Sentinel and in situ measurements to achieve relatively good statistical results in specific conditions. This corresponds to other research in the Netherlands that was able to get good results in this way (Benninga, et al., 2018). The Ksat values that were found show that local circumstances cause this value to change on a local scale, like other research suggests as well (Mahapatra, et al., 2020; Shao & Baumgartl, 2014). Despite the results, there are still points to improve and reflect on in future research. These will be elaborated on in the continuation of this chapter.

6.1 – Comparing in situ and Sentinel soil moisture measurements

The Sentinel-1 satellite provides soil moisture information in a relatively constant way. It provides this info every three days in minimum. Sometimes images cannot be retrieved, limiting the usability to once every six days. This is a high temporal scale compared to manual sampling, but cloudy conditions contribute to the fact that the three day interval is not always achieved.

Sampling soil moisture with semi-permanent soil moisture sensors as was done with the Campbell sensors has the potential to provide a good dataset against which the Sentinel-1 measurements can be validated. Unfortunately, the performance of the Campbell sensors and Sentinel-1 over the course of the study period was not optimal. This is due to a number of reasons:

- The Sentinel-1 satellite measures very high values of soil moisture in the months June to September. The 2019 summer period was dryer than normal and featured a rainfall shortage of 100mm in the end of June up to nearly 200mm in the study area on September 15th, as can be seen in figure 26. This does not stroke with the Sentinel observations indicating a soil moisture content of around 0.35 in the same period compared to an estimated porosity of 0.40-0.45. This effect could be due to vegetation influences on Sentinel. Other research

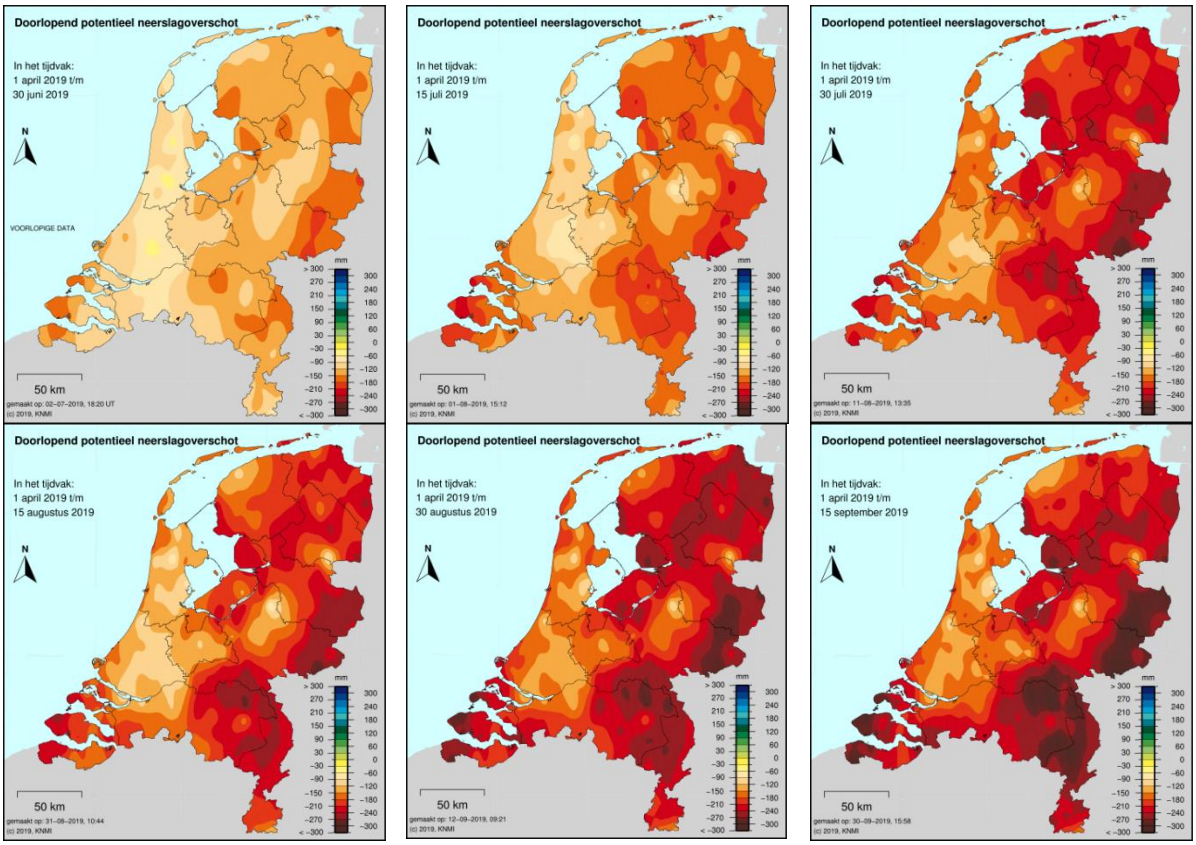

Figure 2610: Developing cumulative rainfall shortage (mm) in the Netherlands during 2019. Top left: June 2nd, top middle: August 1st, top right: August 11th, bottom left: August 31st, bottom middle: September 12th and bottom right: September 30th. Source: KNMI

reports Sentinel being sensitive to crops with a high canopy density and resulting in higher VWC values (Vreugdenhil, et al., 2018);
- The Campbell sensors data contains large data gaps. Measurements done at the southern location (location 1) for example only contained 22 days in the period February-August.

Since most rainfall events that produce erosion and significant runoff occur during the summer, it is crucial that Sentinel soil moisture observations during the summer can be linked to in situ measurements. That way, the satellite can be used to accurately estimate soil moisture content in the catchment at any time. One could argue that the comparison done in this paper is too shallow: why not compare Sentinel to in situ measurements for a year (including winter) or longer? This was not possible due to the data of the Campbell sensors, which roughly cover 2019 and the first month of 2020. Still, there is some data in the months November 2019 – January 2020 which could be used. The outcome could be either positive (correlation between Campbell sensors and Sentinel-1 is found) or negative (no correlation found). In the first case, that would mean that Sentinel observations done during the winter months can accurately be used to predict soil moisture content. Its result would and could not be that all Sentinel measurements throughout the whole year can be used, since the data during growing season shows non-realistic patterns compared to measured data. The next step would be to show the effect of vegetation during winter (think of cover crops) on the Sentinel observations. As mentioned before, this vegetation effect on Sentinel 1 is not worked out yet. This is something future research should aim to solve.

It is, however, possible to use SAR based satellites (of which Sentinel-1 is one) for monitoring of soil moisture content. Studies conducted with the forerunners of Sentinel-1 have demonstrated this (van der Velde, et al., 2012 & Kornelsen & Coulibaly, 2013). Studies done more recently using Sentinel have also proven that Sentinel can be used. These studies also report the not yet solved problem of vegetation during the growing season influencing the Sentinel measurements (Benninga & Pezij, 2019, Carranza et al., 2019, Alexakis et al., 2017 & Gruber et al., 2013).

Statistical tests as done in the results chapter are possible and provide insight into the correlation between two datasets. It is important to realise that the weight of this is relative since the *n* is low, either 15 for location 1 or 30 for location 2 over the span of half a year. A prime example of this is the two outliers in the location 1 correlation data that turn out to influence the outcome of *r* and r^2 a lot. It could be that there seems no relationship now but in fact there is one or vice versa if the number of data points increases. So the statistics do say something, but they don't tell the whole story. In order to do more robust statistical statements, more in situ measurement data is needed. This could also be the reason that the NSE is quite high sometimes whilst other statistical parameters indicate no correlation; maybe NSE is more or less vulnerable to a smaller *n*.

6.2 – High variability in Hydraulic conductivity measurements

Although sampling and measuring Ksat is well documented, it seems tricky to get consistent accuracy in the values. This can be due to a number of reasons. The first reason is that – especially with wet clayish soils – it is important to minimize stress on the soil after taking it from the field. Pressure on the soil could lead to compaction and alter Ksat values of the soil. It is also important to accurately prepare and measure the soil in the lab. Potatoes (that rot over time and when they do so leave large 'gaps' in the sample) and macropores in the soil can lead to higher Ksat values being measured. Both of these phenomenon were encountered in multiple samples. This is in line with other research that is suggesting the impact of vegetation and macropores on Ksat and its spatial variability is way larger than the change that occurs by soil difference (Mahapatra, et al., 2020; Shao & Baumgartl, 2014). Furthermore, there are multiple methods of measuring hydraulic conductivity, which also lead to

different results. Because of time and resource limitations, the method in this paper was chosen. Another method might be more accurate and less prone to large variations (Bakker, Heinen, de Groot, Assinck, & Hummelink, 2018).

6.3 – Modelling reality? Calibration factors

Another point of concern is the working of LISEM as a model and its implementation by the *OpenLisem* software. The software remains a work in progress, where consecutive versions will produce roughly ten times much runoff for the same input. This of course has to be taken into account. Another known issue with LISEM is that water is not flowing through the catchments as quickly as it should. This problem is currently being addressed by the developer of the *OpenLisem* software. This problem where the water is flowing slower than it should is likely to have a huge impact on research related to hydraulic conductivity, like this one. When the water is flowing at a slower speed, it has more time to infiltrate and therefore more water will infiltrate. The effect of measuring hydraulic conductivity as was done in this research can be destroyed when the water flows too slow and too much infiltrates.

Every model has the possibility to calibrate to get to the final result. So does LISEM. The results from the three rainstorms indicate a certain degree to which the modelled and measured outcomes compare. From the graphs it looks like the comparisons between the modelled and observed discharge are not that far off. However, the calibration that was needed to obtain these results was quite big. As can be seen in the results chapter, the two calibration 'buttons' used were the Manning's N and the Ksat multiplication factor.

The Manning's N had to be set to unrealistic low values (order of magnitude 10^{-4}) to obtain the results for both the literature- and manually obtained Ksat values. The Manning's N used is several orders of magnitude smaller than the ones indicated in for example the LISEM manual (Jetten, 2018). Since the Manning's roughness is related to how fast water moves through the catchment, this is likely the correction to the LISEM-related problem of water flowing too slow as described in 8.3. Calibrating in this way it's not entirely possible to solve the problem, because at a certain point the Manning's N values cannot be set lower because of model limitations.

The Ksat multiplication factor had to be set to a very small number to be able to accurately model the discharge to match the recorded discharge from the water board. The values that were used for the manually obtained hydraulic conductivity were not completely unrealistic but were rather low, around 0.4 mm per hour, which is more or less on the low side with what several studies find for this type of soil (Heinen, Bakker, & Wösten, 2018; Wösten, Veerman, & Stolte, 1994). Note that other values such as 20mm/hour are also values that occur in literature, there is large variation within the values that are available. The Ksat values that were obtained from literature are still on the low side for LISEM to get close to the measured output, which can be seen in the multiplication factor Ksat. This factor needed to be set bigger than 1 when working with the literature Ksat values to obtain more or less the same results as the measured runoff. This indicates that the Ksat value for which no calibration is needed, would be around 1.2-1.6mm/hour for farmland and 3.6/4.2mm/hour for grassland. This would bring the hydraulic conductivity close to the 9cm/day (3.75mm/hour) of the Staringreeks (Wösten, Veerman, & Stolte, 1994).

So, calibration was very strong to arrive at somewhat acceptable results and no further calibration was possible due to the very low numbers that LISEM cannot handle. This is also the reason that no numerical (e.g. using NSE) interpretation was given to the LISEM output. This could be done, but the numbers would be somewhat of a façade. For example, say the hydrographs comparison between LISEM and the values measured by the water board would result in an NSE of 0.90 with a Manning's

N and Ksat calibration factor of 0.01, what would this 0.90 tell you? The catchment was modelled in a way not remotely like reality, so this value would lead to misinterpretation of the results.

It could be, however, that newer versions of LISEM, where water flow through the catchment is faster, could yield different results. As a result of faster water flow and less infiltration time, the Ksat values that were measured could yield results that are less far off and need less calibration. Fact is that the current manual measurements of Ksat seem to be orders of magnitude off, something that is unlikely to completely change with faster water flow. It's also good to note that understanding the concepts and relation between connectivity within the catchment and the effect of calibrating with Manning's N and hydraulic conductivity is difficult, since these two factors are very sensitive parameters of the LISEM model (Wei, Dongli, Ming'an, Kwok, & Bingsheng, 2015).

7 Conclusions

7.1 – Comparing satellite and in situ measurements of soil moisture

Statistical analysis of the Sentinel and Campbell data indicates that the two datasets do have no significant correlation. The only weak correlation found (after outliers were excluded) is the Sentinel-1 on location 1 compared to the 20cm soil moisture values on that same location. Table 8 summarizes the results

Table 8: Summary statistics of Sentinel-1 and Campbell data comparison

	Sentinel loc 1 & Campbell loc 1 5cm	Sentinel loc 1 & Campbell loc 1 20cm	Sentinel loc 2 & Campbell loc 2 5cm	Sentinel loc 2 & Campbell loc 2 20cm
R	0.86	0.85	-0.24	-0.04
R^2	0.73	0.72	0.06	0.01
NSE	0.89	0.85	-0.16	0.21
RMSE	0.04	0.05	0.14	0.13

The only comparison between Sentinel and Campbell sensors that has an $R > 0.85$, which in statistics is considered a fairly strong relationship, see (Rumsey, 2009, p.59), is location one with 20cm depth values of soil moisture.

As can be seen in table 8, the RMSE is quite high for the location 2 comparison. This is also what can be seen in the regression graphs in figure 21 (chapter 6), the points are farther apart from the trendline. Points in location 1 are more close to the trendline which indicate better model fit.

To conclude, based on the results the Campbell sensor on location 1 could best be used to calibrate the Sentinel-1 soil moisture content. Especially during the growing season when Sentinel is vulnerable to wrong measurements due to vegetation cover. Unfortunately, the Campbell sensor at location 1 also has the lowest number of observations $(n = 22)$ on a very limited timescale. The other Campbell measurement values and Sentinel data are too far off and are not suitable for this purpose.

7.2 – Measured versus literature based hydraulic conductivity and the effects on model output

The results from the three rain showers as presented in chapter 6 show that it is possible to get reasonably close to measured runoff. Therefore, it is almost impossible to determine a realistic hydraulic conductivity value for this catchment (or soil type within the region of the catchment).

The hydraulic conductivity values of 1mm/hour and 3mm/hour for cropland and grassland respectively as found in the literature seem to get the LISEM model closer to observed runoff. That is, with less dramatic calibration needed. Still, the Manning's N value needs to be set quite low. The value at which little calibration is needed will be somewhere around 1.2-1.6mm/hour for farmland and 3.6-4.2mm/hour for grassland. This is based on the multiplication factor of Ksat that is still needed when considering the literature based values.

Ksat values obtained through manual sampling in this and other studies result in a wider range of values for different land uses compared to literature. At the moment it is only possible to use manually obtained Ksat values to run LISEM with lots of calibration effort. This may improve in the future as the model is further developed.

8 References

Alexakis D., D., K. Mexis, F.-D., Vozinaki, A.-E., Daliakopoulos, I., & Tsanis, I. (2017). Soil moisture content estimation based on Sentinel-1 and auxiliary earth observation products - a hydrological approach. *Sensors*.

Baartman, J. E., Temme, A. J., Veldkamp, T., Jetten, V. G., & Schoorl, J. M. (2013). Exploring the role of rainfall variability and extreme events in long-term landscape development. *Catena*, 25-38.

Bakker, G., Heinen, M., de Groot, W., Assinck, F., & Hummelink, E. (2018). *Hydrofysische gegevens van de bodem in de Basisregistratie Ondergrond (BRO) en het bodemkundig informatie systeem (BIS).* Wageningen: Wageningen University and Research.

Benninga, H., Carranza, C., Pezij, M., Van Santen, P., Van der Ploeg, M., Augustijn, D., & Van der Velde, R. (2018). The Raam regional soil moisture monitoring network in the Netherlands. *Earth System Science Data*, 61-79.

Benninga, H., van der Velde, R., & Su, Z. (2016). Soil moisture retrieval from Sentinel-1 satellite data. *EGU general assembly conference abstracts.*

Benninga, H.-J., & Pezij, M. (2019, March 4). Google Earth Engine tool to generate soil moisture maps with Sentinel-1 satellite imagery. Twente, Netherlands.

Carranza, C., Benninga, H.-J., van der Velde, R., & van der Ploeg, M. (2019). Monitoring agricultural field trafficability using Sentinel-1. *Agricultural water management*.

Comino, J. R., Iserloh, T., Lassu, T., Cerdá, A., Keestra, S. D., Prosdocimi, M., & Sinoga, J. R. (2016). Quantitative comparison of initial soil erosion processes and runoff generation in Spanish and German vineyards. *Science of the total environment*, 1165-1174.

Coulthard, T. J., Hancock, G. R., & Lowry, J. B. (2012). Modeling soil erosion with a downscaled landscape evolution model. *Earth surface processes and landforms*, 1046-1055.

De Roo, A., & Jetten, V. (1999). Calibrating and validating the LISEM model for two datasets from the Netherlands and South Africa. *Catena*, 477-493.

De Roo, A., Offermans, R., & Cremers, N. (1996). LISEM: A single-event, physically based hydrological and soil erosion model for drainage basins. II: Sensitivity analysis, validation and application. *Hydrological Processes*, 1119-1126.

Di Piazza, A., Lo Conti, F., Noto, L., Viola, F., & La Loggia, G. (2011). Comparative analysis of different techniques for spatial interpolation of rainfall data to create a serially complete monthly time series of precipitation for Sicily, Italy. *International Journal of Applied Earth Observatio and Geoinformation*, 396-408.

El Hajj, M., Baghdadi, N., Zribi, M., & Bazzi, H. (2017). Synergic use of Sentinel-1 and Sentinel-2 images for operational soil moisture mapping at high spatial resulotion over agricultural areas. *Remote Sensing*.

Google. (2020, March 22). *Sentinel-1 algorithms*. Retrieved from https://developers.google.com/earth-engine/sentinel1

Gruber, A., Wagner, W., Hegyiova, A., Grefender, F., & Schlaffer, S. (2013). Potential of Sentinel-1 for high resolution soil moisture monitoring. *IGARSS*.

Heinen, M., Bakker, G., & Wösten, J. (2018). *Waterretentie- en doorlatenheidskarakteristieken van boven- en ondergronden in Nederland: de Staringreeks - update 2018.* Wageningen: Wageningen Environmental Research.

Heuvelink, G., Musters, P., & Pebesma, E. (1997). Spatio-temporal Kriging of soil water content. *Geostatistics Wollongong*, 1020-1030.

Hollis, G. E. (1975). The effect of urbanization on floods of different recurrence interval. *Water resources*, 4331-435.

Hornacek, M., Wagner, W., Sabel, D., Truong, H.-L., Snoeij, P., Hahmann, T., . . . Doubková, M. (2012). Potential for higher resolution systematic global surfave soil moisture retrieval via change detection using Sentinel-1. *IEEE Journal of Selected topics in applied earth observations and remote sensing*, 1303-1311.

Hu, W., Shao, M. A., & Si, B. C. (2012). Seasonal changes in surface bulk density and saturated hydraulic conductivity of natural landscapes. *European Journal of Soil Science*, 820-830.

Jain, K. S., & Sudheer, K. P. (2008). *Fitting of hydrological models: a closer look at the Nash-Sutcliffe index.* Journal of hydrologic engineering.

Jetten, V. (2018). *OpenLISEM user manual.* Twente: University of Twente.

Jost, G., Heuvelink, G., & Papritz, A. (2005). Analysing the space-time distributon of soil water storage of a forest ecosystem using spatio-temporal Kriging. *Geoderma*, 258-273.

KNMI. (2020, Januari). *https://cdn.knmi.nl/knmi/map/page/klimatologie/gegevens/maandgegevens/mndgeg_380_tg.txt*.

Kornelsen, K., & Coulibaly, P. (2013). Advances in soil moisture retrieval from synthetic aperture radar and hydrological applications. *Journal of Hydrology*, 460-489.

Kvaerno, S. H., & Stolte, J. (2012). Effects of soil physical data sources on discharge and soil loss simulated by the LISEM model. *Catena*, 137-149.

Lesmes, D. P., Herbstzuber, R. J., & Wertz, D. (1999). Terrain permittivity mapping: GPR measurements of near-surface soil moisture. *Symposium on the Application of Geophysics to engineering and environmental problems* (pp. 575-582). Society of Exploration Geophysicists.

Liu, C. (2016, February). Analysis of Dentinel-1 SAR data for mapping standing water in the Twenthe region. Enschede, The Netherlands.

Lozac'h, L., Baghdadi, N., Al Hajj, M., Zribi, M., & Cresson, R. (2020). Sentinel 1/Sentinel 2 derived soil moisture product at plot scale (S2 MP). *Mediterranean and Middle-East Geoscience and Remote Sensing Symposium*, 168-171.

Mahapatra, S., Jha, M., Biswal, S., & Senapati, D. (2020). Assessing variability of intiltration characteristics and reliability of intfiltration models in a tropical sub-humid region of India. *Scientific reports*.

Meena, R., & Jha, R. (2017). Approximating soil physical properties using geo-statistical models in Lower Kosi basin, Ganga river system, India prone to flood inundation. *International Journal of Civil and Technology*, 1445-1459.

Pandey, A., Himanshu, S. K., Mishra, S. K., & Singh, V. P. (2016). Physically based soil erosion and sediment yield models revisited. *Catena*, 595-620.

Podest, E. (2017). Basics of synthetic aperture radar. *NASA's applied remote sensing training program*, (p. 56).

Rousseau, M., Cerdan, O., Ern, A., Le Maitre, O., & Sochala, P. (2012). Study of overland flow with uncertain infiltration using stochastic tools. *Advances in water resources*, 1-12.

Rumsey, D. (2009). *Statistics for dummies 2.* Indianapolis: Wiley Publishing .

Schoorl, J. M., Veldkamp, A., & Bouma, J. (2002). Modeling water and soil redistribution in a dynamic landscape context. *Soil science society of America*, 1610-1619.

Schouten, C. J., Rang, M. C., & Huigen, P. M. (1985). Erosie en wateroverlast in Zuid-Limburg. *Landschap*, 118-132.

Shao, Q., & Baumgartl, T. (2014). Estimating input parameters for four infiltration models from basic soil, vegetation and rainfall properties. *Soil Physics*.

Sheikh, V., van Loon, E., Hessel, R., & Jetten, V. (2010). Sensitivity of LISEM predicted catchment discharge to initial soil moisture content of soil profile. *Journal of hydrology*, 174-185.

Smith, R., Goodrich, D., & Unkrich, C. (1999). Simulation of selected events on the Catsop catchment by KENEROS2 - a report for the GCTS conderence on catchment scale models. *Catena*, (p. 19).

Snepvangers, J., Heuvelink, G., & Huisman, J. (2003). Soil water content interpolation using spatio-temporal kriging with external drift. *Geoderma*, 252-271.

Stolte, J. (1997). *Manual for soil physical measurements: version 3'.* DLO Winand Starting Centre.

van der Velde, R., Su, Z., van Oevelen, P., Wen, J., Ma, Y., & Salama, S. (2012). Soil moisture mapping over the central part of the Tibetan Plateau using a series of ASAR WS images. *Remote Sensing of Environment*, 175-187.

Vreugdenhil, M., Wolfgang, W., Bauer-Marchallinger, B., Isabell, P., Irene, T., Christoph, R., & Strauss, P. (2018). Sensitivity of Sentinel-1 Backscatter to vegetation dynamics: An Austrian study. *Remote seneing*.

Wei, H., Dongli, S., Ming'an, S., Kwok, P., & Bingsheng, S. (2015). Effects of initial soil water content and saturated hydraulic conductivity variability on small watershed runoff simulation using LISEM. *Hydrologogical sciences journal*, 1137- 1154.

Winteraeken, H. J., & Spaan, W. P. (2010). A new approach to soil erosion and runoff in South Limburg - the Netherlands. *Land degradation & development*, 346-352.

Wösten, H., de Vries, F., Hoogland, T., Massop, H., Veldhuizen, A., Vroon, H., . . . Bolman, A. (2013). *BOFEK2012, de nieuwe, bodemfysische schematisatie van Nederland.* Wageningen: Alterra, WUR.

Wösten, J., Veerman, G., & Stolte, J. (1994). *Waterretentie- en doorlatendheidskarakteristieken van boven- en ondergronden in Nederland: de Staringreeks.* Wageningen: DLO-Staring Centrum.

Annex 1 – The Sentinel-1 soil moisture script

```
//Basic settings

var EXPORT_image = true;

var EXPORT_table = false;

var MOSAIC = true;

var SAT_5cm = ee.Image("users/hjbenninga/BOFEK2_1_VGE_SAT_5cm");

var WP_5cm = ee.Image("users/hjbenninga/BOFEK2_1_VGE_WP_5cm");

Map.centerObject(catsop, 14);

var SCALE = 5;          //scale [meter] of exported image and table

var Area = catsop;          //area over which statistics are calculated

var Area_small = catsop;  //area that is covered with imagery in the output

var Date_image = ee.Date('2019-05-26T00:00:00');


//LOADING OF SENTINEL-1

//Load Sentinel-1 C-band SAR ground range collection (log scaling, VV co-polar)

var collection_S1_TOTAL = ee.ImageCollection('COPERNICUS/S1_GRD').filterBounds(Area)

  .filter(ee.Filter.listContains('transmitterReceiverPolarisation','VV'))

  .filter(ee.Filter.eq('instrumentMode','IW'))

  .filterDate('2016-01-01', Date.now())

  .filter(ee.Filter.eq('resolution_meters', 10));

var collection_S1_STATS = collection_S1_TOTAL.filterDate('2016-01-01','2020-03-04'); //statistics are
calculated over the selected time period


//INCIDENCE ANGLE CORRECTION

var n=2;                //normalization coefficient

var angle_ref = 37.5;   //reference angle


//define incidence angle correction function

var incidence_angle_correction_function = function(image) {

  var image_m2m2 = image.expression(

    '10**(image/10)',{
```

```
    'image': image.select('VV')
   });

  var image_m2m2_cor = image_m2m2.expression(
   'sigma0*((cos(pi/180*angle_ref)**n)/(cos(pi/180*angle)**n))',{
    'n': n,
    'angle_ref': angle_ref,
    'sigma0': image_m2m2,
    'angle': image.select('angle'),
    'pi': Math.PI
   });

  var output_image = image_m2m2_cor.expression(
   'log10(sigma0_cor)*10', {
    'sigma0_cor': image_m2m2_cor
   });

  return output_image.set('system:time_start',
image.get('system:time_start'));
};

//apply incidence angle correction function
var collection_S1_STATS_IC_cor = collection_S1_STATS.map(incidence_angle_correction_function);
var collection_S1_TOTAL_IC_cor = collection_S1_TOTAL.map(incidence_angle_correction_function);

//MASK SENTINEL-1: VALID OBSERVATION VALUES
var min_value = -20;
var max_value = -2;
var min_coverage_ratio = 0.75;
```

```
//Define making function
var valid_values_mask_function = function(image) {
  var lower_mask = image.gte(min_value);
  var new_img = image.updateMask(lower_mask);

  var upper_mask = new_img.lte(max_value);
  var new_img2 = new_img.updateMask(upper_mask);

  return new_img2.set('system:time_start',
image.get('system:time_start'));
};

//apply threshold values to image collections
var collection_S1_STATS_IC_cor = collection_S1_STATS_IC_cor.map(valid_values_mask_function);
var collection_S1_TOTAL_IC_cor = collection_S1_TOTAL_IC_cor.map(valid_values_mask_function);

//MASK SINTINEL-1 : COVERAGE OF A PIXEL
//Determine ratio of images
var count_collection_TOTAL = collection_S1_TOTAL_IC_cor.reduce(ee.Reducer.count());
var count_collection_TOTAL_masked = collection_S1_TOTAL_IC_cor.reduce(ee.Reducer.count());
var count_collection_STATS = collection_S1_STATS_IC_cor.reduce(ee.Reducer.count());
var count_collection_STATS_masked = collection_S1_STATS_IC_cor.reduce(ee.Reducer.count());

var valid_coverage_STATS_ratio = count_collection_STATS_masked.divide(count_collection_STATS);
var valid_coverage_TOTAL_ratio = count_collection_TOTAL_masked.divide(count_collection_TOTAL);

//Apply filter of min_coverage_ratio
var collection_S1_STATS_IC_cor_Masked2 = collection_S1_STATS_IC_cor.map(function(img) {
  var mask = valid_coverage_STATS_ratio.gte(min_coverage_ratio);
  var new_img = img.updateMask(mask);
  return new_img;});
```

```
//CHANGE DETECTION STATISTICS

collection_S1_STATS_IC_cor_Masked2.reduce(ee.Reducer.max()); // Maximum in each pixel

collection_S1_STATS_IC_cor_Masked2.reduce(ee.Reducer.min()); // Minimum in each pixel

//Get stats as input to change detection

var max_collection = collection_S1_STATS_IC_cor_Masked2.reduce(ee.Reducer.percentile([97.5]));
//97.5% percentile to exclude outliers

var min_collection = collection_S1_STATS_IC_cor_Masked2.reduce(ee.Reducer.percentile([2.5]));
//2.5% percentile to exclude outliers


//RETRIEVE A RELATIVE SOIL MOISTURE INDEX

//define change detection function

var change_detection_function = function(image) {

 var output_image = image.expression(

   '(s1_im - s1_min)/(s1_max - s1_min)',{

     's1_im': image,

     's1_min':min_collection,

     's1_max': max_collection,

 });

 return output_image.set('system:time_start',

 image.get('system:time_start'));

 };


//apply change detection

var cd_s1 = collection_S1_TOTAL_IC_cor.map(change_detection_function);

//cd_s1 indicates the relative saturation of the soil as a value between 0 and 1


//RETRIEVE VOLUMETRIC SOIL MOISTURE

var WP_SAT_scale_function = function(image) {

 var output_image = image.expression(

   '(MAX - MIN) * index + MIN', {

     'index': image,

     'MIN': WP_5cm,
```

```
    'MAX': SAT_5cm, });


return output_image.set('system:time_start', image.get('system:time_start'));};


//Apply scaling between WP and SAT

var cd_s1_volumetric = cd_s1.map(WP_SAT_scale_function);

print(cd_s1_volumetric,'Image collection of volumetric soil moisture maps');


//CD_S1_volumetric map

//Map.addLayer(cd_s1_volumetric);


//MAPS AND GRAPHS

//Map display - mosaic images on same day that cover Area_small

if (MOSAIC === true) {

  var date_object =
ee.Date(ee.Image(cd_s1_volumetric.filterDate(Date_image,Date.now()).filterBounds(Area_small).firs
t()).get('system:time_start'));

  var cd_s1_volumetric_date =
ee.ImageCollection(cd_s1_volumetric.filterDate(date_object,date_object.advance(1,'day')).filterBou
nds(Area_small)); //select images that cover area of interest on/after date image

  var image1 =  ee.Image(cd_s1_volumetric_date.first());

  var date_image1 = ee.Date(image1.get('system:time_start'));

  var cd_s1_volumetric_date_image = cd_s1_volumetric_date.mosaic().set('system:time_start',
date_image1);

  var cd_s1_volumetric_date_image_Study_area = cd_s1_volumetric_date_image.clip(Area_small); //
Clip to image to area of interest

  print(cd_s1_volumetric_date_image_Study_area,'Mosaiced image covering the area of interest on
date of interest');

  print(cd_s1_volumetric_date_image,'Mosaiced image covering the area of interest on date of
interest');

} else {

  var cd_s1_volumetric_date_image =
ee.Image(cd_s1_volumetric.filterDate(Date_image,Date.now()).filterBounds(Area_small).first());
//Select first image that covers area of interest on/after Date_image
```

```
  var cd_s1_volumetric_date_image_Study_area = cd_s1_volumetric_date_image.clip(Area_small); // Clip to image to area of interest

  print(cd_s1_volumetric_date_image_Study_area,'First image covering the area of interest on date of interest');}


//ADD LAYERS TO MAPS

Map.centerObject(catsop, 14);

Map.addLayer(SAT_5cm, {minL:0, max:0.7, opacity:1, palette: ['ff1c05', 'fff705','4dff03','07ffe8','0501ff']}, 'saturation soil moisture [m^3/m^3'); //Add map with saturation soil moisture

Map.addLayer(WP_5cm, {min: 0, max: 0.7, opacity:1, palette: ['ff1c05', 'fff705','4dff03','07ffe8','0501ff']}, 'Wilting point soil moisture [m^3/m^3]'); // Add map with wilting point soil moisture

var valid_coverage_ratio_Study_area = valid_coverage_STATS_ratio.clip(Area_small);

Map.addLayer(valid_coverage_ratio_Study_area, {min: 0, max: 1, opacity: 1, palette: ['LightBlue','blue']}, 'Ration of valid values');


//map soil moisture image

Map.addLayer(cd_s1_volumetric_date_image_Study_area, {min: 0, max: 0.7, opacity:1,palette: ['ff1c05', 'fff705','4dff03','07ffe8','0501ff']}, 'Volumetric soil moisture [m^3/m^3]');


//Plot figure soil moisture in time

var SoilMoisture_mean_TimeSeries = ui.Chart.image.series(cd_s1_volumetric, Area_small, ee.Reducer.mean(), SCALE).setOptions({

  hAxis: {title:'Date'},

  vAxis: {title:'Volumetric soil moisture'}  });

print(SoilMoisture_mean_TimeSeries,'Time series of mean soil moisture for the area of interest');

var SoilMoisture_count_TimeSeries = ui.Chart.image.series(cd_s1_volumetric, Area_small, ee.Reducer.count(), SCALE).setOptions({

  hAxis:{title:'Date'},

  vAxis:{title:'Number of pixels'}});

print(SoilMoisture_count_TimeSeries,'Time series of number of pixels for the area of interest');
```

```
//EXPORT A TABLE AND IMAGE

var date_object = ee.Date(cd_s1_volumetric_date_image_Study_area.get('system:time_start'));

var date_string = date_object.format('YYYYMMdd_HHmm');

if (EXPORT_table === true) { //// From: https://gis.stackexchange.com/questions/274569/exporting-table-in-to-a-drive-from-google-earth-engine-returns-blank-rows

  var cd_s1_volumetric_Area_small = ee.ImageCollection(cd_s1_volumetric.filterBounds(Area_small)); // Select images that cover area of interest

  var reducers = ee.Reducer.mean().combine({ //combine the mean and count

    reducer2: ee.Reducer.count(),

    sharedInputs: true

  });

  var Region_table = cd_s1_volumetric_Area_small.map(function(img) {

    return img.reduceRegions({

      collection: Area_small,

      reducer: reducers,

      scale: SCALE

    }).map (function(f){

      return f.set('Date', ee.Date(img.get('system:time_start')));

    });

  }).flatten();

  print(Region_table.limit(20),'Feature table: first # elements in time series');

  Export.table.toDrive({

    collection: Region_table,

    description: 'ResultsTable_area_of_interest' + date_string.getInfo(),

    selectors:(['Date','Mean','Count']),

    });

    print('See tab Tasks to start exporting a table with mean and number of pixels for area of interest');

}

else {

  print('No table export (see variable EXPORT table');

}
```

```
//Export the image
print('Timestamp image: ', date_string);
if(EXPORT_image === true) {
  Export.image.toDrive({
    image: cd_s1_volumetric_date_image_Study_area,
    description: 'Vol_SoilMoisture' + date_string.getInfo(),
    scale: SCALE, //In meters, specified in line 11
  region: Area_small
  });
  print('See tab Tasks to start exporting a soil moisture map for area of interest');
} else {
  print('No image export (see variable EXPORT_image)');
  }
```

Annex 2 – November fieldwork layout form

General

Date	
Time	
Sample location	
Sample number	

TDR measurements	First	Second	Third
Values at point 1			
Values at point 2			
Values at point 3			
Values at point 4			

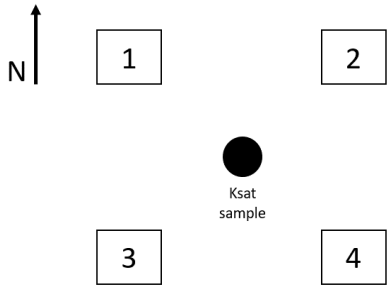

Annex 3 – The PCraster script

```
#comments start with a hashtag
#! --matrixtable --lddin --clone clone.map
#####################################################
# PCRASTER script to build a LISEM input database #
# made by Meindert Commelin 06/02/2019          #
#####################################################
binding
##################
### INPUT MAPS ###
##################
dem = dem.map; # digital elevation model, area must be <= clone
lu = lu.map; # field id's for land use
# roads = roads.map; # location of roads value = 1
# grass = grasswid.map; # only if buffers are included
surface = catch.map; # field id's for texture/soil map
# chanmask = chanmask.map; # location of channels value = 1 (optional)
####################
### INPUT TABLES ###
####################
# There are two tables which combine with either land use or soil/geology.
# Choose for each of the following 15 parameters in which table it belongs.
# renumber the paramaters for each table (see example basic script)
# unittblsoil = surface.txt;
# table with soil parameters for each field id
unittbl = lookup_tbl.txt;
# table with crop and land use parameters for each field id
#
# 01 rr (cm) = random roughness
# 02 n = Manning's n
# 03 stonefraction (ratio)
# 04 coh (kPa) = cohesion of soil
# 05 aggregate stability (number)
# 06 D50 (µm)
# 07 ksat (mm/h)
# 08 psi initial (cm)
# 09 thetas (cm3/cm3) = porosity
# 10 thetai (cm3/cm3) = initial moisture content
# 11 soildepth (cm)
# 12 per (fraction) = surface cover by vegetation
# 13 lai (m2/m2) = leaf area index
# 14 ch (m) = crop height
# 15 cohadd (kPa) = additional cohesion by roots
########################
### INPUT CONSTANTS ###
########################
# channel properties:
# NOTE: if channels with different parameters, use a table as with land use.
# Chanwidth = 2; # width of channels in meters
# Chanside = 0; # tan of angle between side and surface (0 = rectangular)
# Chanman = 0.2; # Manning's n in channel
```

```
# Chancoh = 10; # high cohesion, kPa
# ChanKsat = 20; # channel ksat for infiltration
# roads:
# widthroads = 6; # width of roads in meters
####################
### PROCES MAPS ###
####################
area = area.map; # value = 1
####################
### OUTPUT MAPS ###
####################
### rainfall map ###
rain_id = id.map; # only if >1 rainfall zones --> not needed I assume
### basic topography related maps ###
grad = grad.map; # slope gradient
Ldd = ldd.map; # Local Drain Direction
outlet = outlet.map; # location outlets and checkpoints
outpoint = outpoint.map; # outlet points subcatchments
### land use maps ###
per = per.map; # surface cover by vegetation
lai= lai.map; # leaf area index
ch = ch.map;  # crop height
roadwidth = roadwidth.map;
# grass = grasswid.map; # width of grass strips (optional)
# smax = smax.map; # max canopy storage (optional)
### surface maps ###
rr = rr.map; # random roughness
mann = n.map; # Manning's n
stone = stonefrc.map; # stone fraction
# crust= crustfrc.map; # crusted fraction of surface (optional)
# comp = compfrc.map; # compacted fraction of surface (optional)
# hard = hardsurf.map; # impermeable surface (optional)
### erosion maps ###
coh = coh.map; # cohesion of the soil
cohadd = cohadd.map; # additional cohesion by roots
aggrstab = aggrstab.map; # aggregate stability
D50 = d50.map; # median texture size
### infiltration maps ###
# for G&A 1st layer:
ksat= ksat1.map;
psi= psi1.map;
pore= thetas1.map;
thetai= thetai1.map;
thetas= thetas1.map;
soildep= soildep1.map;
# for G&A 2nd layer: (optional)
# ksat2= ksat2.map;
# psi2= psi2.map;
# pore2= thetas2.map;
# thetai2= thetai2.map;
# soildep2= soildep2.map;
### channel maps ### (optional)
```

```
# lddchan = lddchan.map;
# chanwidth = chanwidt.map;
# chanside = chanside.map;
# changrad = changrad.map;
# chanman = chanman.map;
# chancoh = chancoh.map;
### channel infiltration ### (optional)
# chanksat = chanksat.map;
initial
####################
### PROCESS MAPS ###
####################
area = dem * 0 + 1;
############################
### MAPS WITH RAINFALL  ###
############################
report rain_id = area; # only 1 rainfall zone
# for >1 rainfall zones based on points use ArcGIS or:
# report id = spreadzone(points, 0, friction);
# with; points = boolean map with locations of rainfall stations
# and friction = friction map (see page 70 of LISEMdocumentation6)
#################
### BASE MAPS ###
#################
report grad = max(sin(atan(slope(dem))),0.001);
report Ldd = lddcreate(dem, 1e20,1e20,1e20,1e20); # correct topo for local depressions #
report outlet = pit(Ldd);
report outpoint = pit(Ldd);
######################
### LAND USE MAPS ###
######################
report per = lookupscalar(unittbl, 12, lu); # fraction soil cover
report ch = lookupscalar(unittbl, 14, lu); # crop height (m)
# choose method for lai:
report lai = lookupscalar(unittbl, 13, lu); # leaf area index
# or: (explained on page 71-72 from LISEMdocumentation6_170215)
# per = min(per, 0.95);
# lai = ln(1-coverc)/-0.4;
# report lai = if(per gt 0, lai/per, 0); # leaf area index
####################
### SURFACE MAPS ###
####################
report rr = lookupscalar(unittbl, 1, lu); # random roughness (=std dev in cm)
report mann = lookupscalar(unittbl, 2, lu); # Manning's n
# report mann = 0.051*rr+0.104*per; # or use simple regression from Limburg data: CAREFULL this is
not published
report stone = lookupscalar(unittbl, 3, lu); # stone fraction
# report roadwidth = roads * scalar(widthroads);
####################
### EROSION MAPS ###
####################
report coh = lookupscalar(unittbl, 4, lu);
```

```
report cohadd = lookupscalar(unittbl, 15, lu);
report aggrstab = lookupscalar(unittbl, 5, lu);
report D50 = lookupscalar(unittbl, 6, lu);
########################################
### INFILTRATION MAPS for GREEN & AMPT ###
########################################
report ksat = lookupscalar(unittbl, 7, lu);
report psi = lookupscalar(unittbl, 8, lu);
report thetas = lookupscalar(unittbl, 9, lu);
report thetai = lookupscalar(unittbl, 10, lu);
report soildep = lookupscalar(unittbl, 11, lu);
# report ksat2 = lookupscalar(unittbl[name], [col.nr], [map.name]);
# report psi2 = lookupscalar(unittbl[name], [col.nr], [map.name]);
# report thetas2 = lookupscalar(unittbl[name], [col.nr], [map.name]);
# report thetai2 = lookupscalar(unittbl[name], [col.nr], [map.name]);
# report soildep2 = lookupscalar(unittbl[name], [col.nr], [map.name]);
####################
### CHANNEL MAPS ###
####################
# report lddchan= lddcreate(dem*chanmask,1e20,1e20,1e20,1e20);
# report chanwidth=chanmask*scalar(Chanwidth);
# report chanside=chanmask*scalar(Chanside);
# report changrad=max(0.001,sin(atan(slope(chanmask*dem))));
# report chanman=chanmask*scalar(Chanman);
# report chancoh=chanmask*scalar(Chancoh);
############################
### CHANNEL INFILTRATION ###
############################
# report chanksat = chanmask*scalar(ChanKsat);
```

Annex 4 – Rainfall files used for LISEM runs

March 15th rainfall file

T (min)	I(mm/h)						
		28	12	56	0	84	0
1	24	29	12	57	0	85	0
2	24	30	12	58	0	86	0
3	24	31	12	59	0	87	0
4	24	32	0	60	12	88	12
5	24	33	12	61	0	89	0
6	36	34	12	62	0	90	12
7	24	35	0	63	0	91	0
8	36	36	12	64	0	92	0
9	24	37	0	65	12	93	12
10	18	38	0	66	0	94	0
11	18	39	0	67	0	95	12
12	18	40	12	68	0	96	12
13	18	41	0	69	12	97	12
14	18	42	0	70	0	98	12
15	18	43	0	71	0	99	12
16	18	44	0	72	0	100	12
17	18	45	0	73	0	101	12
18	18	46	0	74	0	102	12
19	18	47	0	75	0	103	12
20	18	48	12	76	0	104	12
21	18	49	0	77	0	105	12
22	12	50	0	78	0	106	12
23	12	51	0	79	0	107	12
24	12	52	0	80	0	108	12
25	12	53	0	81	0	109	12
26	12	54	12	82	0	110	24
27	12	55	0	83	0	111	12

112	12	143	0	174	0	205	0
113	24	144	0	175	0	206	0
114	12	145	0	176	0	207	0
115	12	146	0	177	0	208	0
116	24	147	0	178	0	209	0
117	12	148	0	179	0	210	0
118	12	149	0	180	0	211	0
119	24	150	0	181	0	212	0
120	12	151	0	182	0	213	0
121	12	152	0	183	0	214	0
122	12	153	0	184	0	215	0
123	0	154	0	185	0	216	0
124	0	155	0	186	0	217	0
125	12	156	12	187	0	218	0
126	0	157	0	188	0	219	0
127	0	158	0	189	0	220	0
128	12	159	0	190	0	221	0
129	0	160	0	191	0	222	0
130	0	161	0	192	0	223	0
131	0	162	0	193	0	224	0
132	0	163	0	194	12	225	0
133	0	164	0	195	0	226	0
134	0	165	0	196	0	227	12
135	0	166	12	197	0	228	0
136	0	167	0	198	0	229	0
137	12	168	0	199	0	230	0
138	0	169	0	200	0	231	0
139	0	170	0	201	0	232	0
140	0	171	0	202	0	233	0
141	0	172	0	203	0	234	0
142	0	173	0	204	0	235	0

236	0	238	0	240	0
237	0	239	0	241	12

May 28th rainfall file

T (min)	I(mm/h)						
		24	0	50	0	76	0
		25	12	51	0	77	0
0	0	26	0	52	0	78	0
1	0	27	0	53	12	79	0
2	12	28	0	54	0	80	0
3	12	29	12	55	0	81	0
4	12	30	0	56	0	82	0
5	24	31	0	57	0	83	0
6	24	32	0	58	0	84	0
7	24	33	0	59	0	85	0
8	12	34	12	60	0	86	0
9	0	35	0	61	0	87	0
10	0	36	0	62	0	88	0
11	0	37	0	63	0	89	0
12	0	38	12	64	12	90	0
13	0	39	0	65	0	91	0
14	0	40	0	66	0	92	12
15	12	41	0	67	0	93	0
16	12	42	0	68	0	94	0
17	24	43	0	69	0	95	0
18	24	44	0	70	0	96	0
19	12	45	0	71	0	97	0
20	24	46	0	72	0	98	0
21	0	47	12	73	0	99	0
22	12	48	0	74	0	100	0
23	0	49	0	75	0		

September 29th rainfall file

T (min)	I(mm/h)						
1	12	12	0	23	0	34	0
2	0	13	12	24	0	35	0
3	0	14	12	25	0	36	0
4	0	15	0	26	0	37	0
5	0	16	12	27	0	38	0
6	12	17	0	28	12	39	0
7	0	18	12	29	0	40	0
8	12	19	24	30	0	41	0
9	24	20	72	31	0	42	0
10	12	21	12	32	0		
11	12	22	0	33	0		